Original Study **Open Access**

Litan Debnath, S.M. ASCE*

Seismic bearing capacity of shallow strip footing embedded in slope resting on two-layered soil

https://doi.org/10.2478/sgem-2021-0021
Received December 15, 2020; accepted June 20, 2021

Abstract: In this paper,the limit equilibrium method with the pseudo-static approach is developed in the evaluation of the influence of slope on the bearing capacity of a shallow foundation. Particle swarm optimisation (PSO) technique is applied to optimise the solution. Minimum bearing capacity coefficients of shallow foundation near slopes are presented in the form of a design table for practical use in geotechnical engineering. It has been shown that the seismic bearing capacity coefficients reduce considerably with an increase in seismic coefficient. Besides, the magnitude of bearing capacity coefficients decreases further with an increase in slope inclination.

Keywords: Pseudo-static, Particle swarm optimisation, Bearing capacity coefficient, Slope inclination, Limit equilibrium

1 Literature Review

Many researchers analysed the bearing capacity based on the static method in which the bearing capacity coefficients were calculated based on static loads on the footings and the weight of the soil in both active and passive conditions. The classical bearing capacity theories started from Rankine (1857), Prandtl (1921), Terzaghi (1943), Meyerhof (1957), Saran et al. (1989) and many others who extensively studied the bearing capacity of shallow footings for static loading case. Terzaghi's bearing capacity theory (1943) was the first general theory for the bearing capacity of soils. Okabe (1924) and Mononobe and Matsuo (1929) were the pioneers in the inclusion of 'seismicity' in the design of structures. IS: 1893-1984(Part-3) has also adopted the Mononobe and Okabe method for the determination of seismic active and passive earth pressure behind the retaining wall. Sarma and lossifelis (1990), Richards et al. (1993), Budhu and Al-Karni (1993) and Kumar and Kumar (2003) considered the seismic forces both on the structures and on the supporting soil mass, which were not considered by Meyerhof (1957). Researchers like Dormieux and Pecker (1995), Paolucci and Pecker (1997), Soubra (1997), Kumar and Rao (2002), Kumar (2003) and Choudhury and Subba Rao (2005) studied the seismic bearing capacity of shallow footings for horizontal ground. Sawada et al. (1994), Sarma (1999) and Askari and Farzaneh (2003) gave the solution for seismic bearing capacity of shallow foundations near the sloping ground. Again, some work for surface footing on the sloping ground was carried out by Zhu (2000), Kumar and Kumar (2003) and Kumar and Rao (2003) using limit equilibrium analysis, method of characteristics, etc. Choudhury and Rao (2006),Castelli and Lentini (2012), Farzaneh and Askari (2013) and Chakraborty and Kumar (2014) determined the seismic bearing capacity of a shallow foundation embedded in sloping ground by using the theorem of limit equilibrium method and limit analysis in conjunction with finite elements and non-linear optimisation technique, respectively.In their analysis, it was found that on increasing slope inclination, the bearing capacity decreased. But the researchers did not analyse the bearing capacity on layered soil.Yamamoto (2010) investigated seismic bearing capacity coefficients of spread and embedded foundations near slope in the analytical method. The pseudo-static approach was used, and the seismic forces consisted of a horizontal load applied to the foundation and inertia of a soil mass. Chakraborty and Kumar (2013) evaluated the bearing capacity factor on the sloping ground by applying lower bound (LB) finite element limit analysis in conjunction with non-linear optimisation. Baazouzi et al. (2016) studied the numerical analysis of the bearing capacity for a strip footing near a cohesionless slope and subjected to a centred load using the finite difference code. Button (1953) was the first to analyse the bearing capacity of strip footing on two layers of clay under static loading conditions. In this analysis, it was postulated that failure surface at the ultimate load is cylindrical, where the centre of the cylindrical curve lies at the edge of the footing.

***Corresponding Author: Litan Debnath, S.M. ASCE:** Research Scholar, Civil Engineering Department, National Institute of Technology Agartala, PIN-799046, INDIA, E-mail: litandbnth4@gmail.com

Meyerhof and Hanna (1978) considered the case of footing reposing in various layers overlaying a strong soil deposit. Michalowski and Shi (1995) applied the kinematic approach of limit analysis to account for the limit pressure under footings to ascertain the bearing capacity of footings reposing on two-layered soil. Purushothamaraj et al. (1974) analysed the bearing capacity of shallow substratum utilising the upper bound (UB) limit analysis theorem. From all these literature surveys, it is seen that the bearing capacity of shallow foundation embedded in slope on layered soil is still limited. In the present analysis,the seismic bearing capacity of strip footing embedded in slope on two-layered soil has been analysed by using the limit equilibrium method with the pseudo-static approach.

2 Methodology

A strip footing having a width B_0 is assumed to be on the top of a two-layered $c-\phi$ soil as shown in Fig. 1. The footing (Fig. 2) having base AM is embedded in a sloping ground DY with an inclination i to the horizontal ground surface. The footing is resting on two-layered c-ϕ soil. Homogeneous, isotropic c-ϕ soil with surcharge load along with the sloping ground is assumed in the analysis. Soil is assumed to be a rigid, perfectly plastic medium satisfying the Mohr–Coulomb failure criterion.Let the footing be at a depth of (D_f) below the ground surface (Fig. 2). Load (P_I) acts along the centre line of the footing. For shallow foundation ($D_f \leq B_0$), the overburden pressure is idealised here as a triangular load distributionthat acts over the length of RY at an angle of inclination (i). From the concept of Debnath and Ghosh (2018), the two main regions, active wedge and passive wedge, are thereby assumed to be acoulomb failure mechanism as shown in Fig. 2. The active region gives an active lateral thrust P_A pushing against the passive resistance P_p. The wall frictional angle between the active and passive zones is denoted as δ. The active and passive zones are inclined at an angle α_{A1}, α_{A2}, α_{p1} α_{p2}, respectively. The detailed free body diagram of the active zone and passive zone is shown in Figs 3–6. From the equilibrium of the two wedges, the active pressure and passive resistance will be equal. Then, by equating the active pressure and passive resistance, the authors found out the maximum load acting on the foundation. After optimisation of the load p_L by particle swarm optimisation (PSO) technique, the authors found out the minimum resistance. Parameters involved in the present study are as follows:
c_1= cohesion of soil in the top layer, c_2= cohesion of soil in the bottom layer, ϕ_1 = angle of friction of soil in the top layer, ϕ_2= angle of friction of soil in the bottom layer, γ_1= unit weight of soil in the top layer, γ_2= unit weight of soil in the bottom layer, α_{A1} = angle of slip surface at the top layer in the active zone, α_{A2} = angle of slip surface at the bottom layer in the active zone, α_{p1} = angle of slip surface at the top layer in the passive zone, α_{p2} = angle of slip surface at the bottom layer in the passive zone, δ_i= friction angle along the surface between active and passive zones at the i^{th} layer.

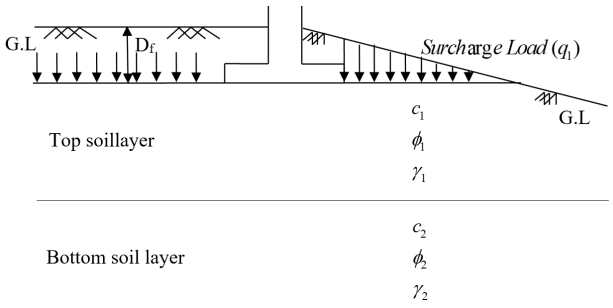

Figure 1: Geometry of footing on two-layered soil profile.

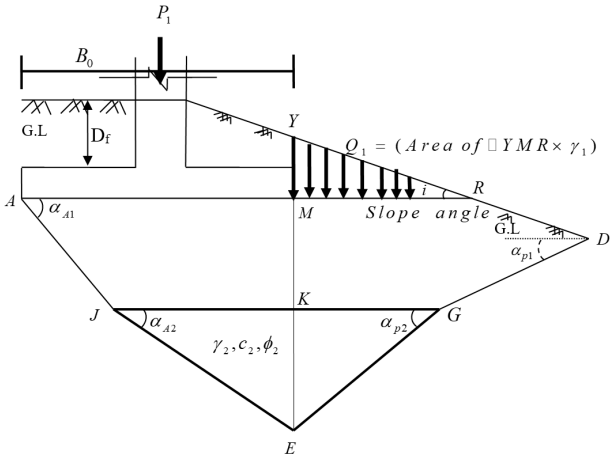

Figure 2: Failure mechanism and wedges assumed in present analysis.

2.1 Active pressure at the top layer

As shown in Fig. 3, wedge AMKJ is a known active wedgethat is posited at the top layer, giving pressure to the passive wedge. The weight of the wedge

$$W_A = \frac{2B_0 - h_1 \cot \alpha_{A1}}{2} h_1 \gamma_1,$$

with the length of JK being equal to

$$(B_0 - h_1 \cot \alpha_{A1}) \tag{1}$$

Total load acting on the foundation is given by

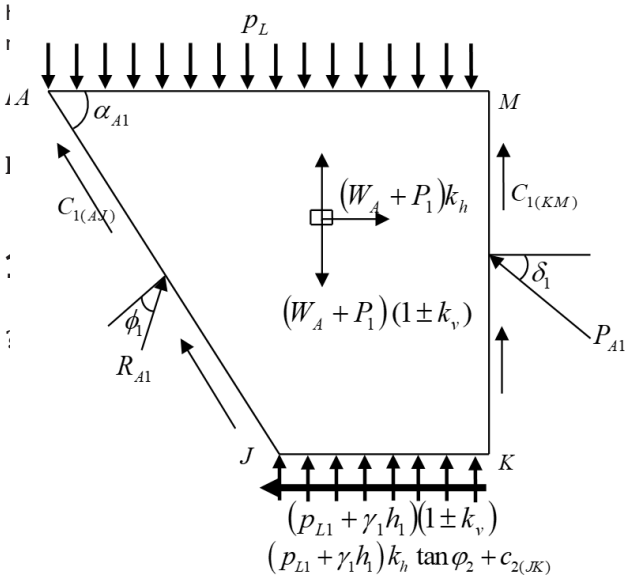

Figure 3: Active wedge in Top layer.

$$P_1 = p_L B_0 \tag{2}$$

Total cohesive force (C_1) on the slip lines AJ and MK is calculated as

$$\begin{aligned} &C_{1(MK)} = c_1 h_1,\ C_{1(AJ)} = c_1 AJ = c_1 h_1 \cos ec\alpha_{A1} \\ &C_{2(JK)} = c_2 JK = c_2 (B_0 - h_1 \cot\alpha_{A1}) \end{aligned} \tag{3}$$

The intensity of load at layer thickness h_1 is expressed as (depicted in Fig. 7)

$$p_{L1} = \frac{p_L B_0}{(B_0 + h_1)} \tag{4}$$

Conceding to limit equilibrium conditions, the authors can write

$$\sum V = 0$$

$$\begin{aligned} &\Rightarrow C_{1(AJ)} \sin\alpha_{A1} + C_{1(MK)} + R_{A1} \cos(\alpha_{A1} - \phi_1) + \\ &+ P_{A1} \sin\delta_1 + (p_{L1} + \gamma_1 h_1) JK (1 - k_v) - \\ &- (P_1 + W_A)(1 - k_v) = 0 \end{aligned} \tag{5}$$

$$\sum H = 0$$

$$\begin{aligned} &\Rightarrow -C_{1(AJ)} \cos\alpha_{A1} + R_{A1} \sin(\alpha_{A1} - \phi_1) - P_{A1} \cos(\delta_1) - \\ &- \{(p_{L1} + \gamma_1 h_1) JK k_h \tan\phi_2 + c_{2(JK)} JK\} + \\ &+ (P_1 + W_A) k_h = 0 \end{aligned} \tag{6}$$

After solving Equations 5 and 6 and modifying both,the active pressure can be obtained as given below:

$$\begin{aligned} P_{A1} = {} & p_L B_0 \left\{ \frac{(1 - k_v)\sin(\alpha_{A1} - \phi_1) + k_h \cos(\alpha_{A1} - \phi_1)}{\cos(\alpha_{A1} - \phi_1 - \delta_1)} \right\} \\ & - \left\{ \frac{p_L B_0}{(B_0 + h_1)} (B_0 - h_1 \cot\alpha_{A1}) \right\} \\ & \left\{ \frac{(1 - k_v)\sin(\alpha_{A1} - \phi_1) + k_h \tan\phi_2 \cos(\alpha_{A1} - \phi_1)}{\cos(\alpha_{A1} - \phi_1 - \delta_1)} \right\} + \\ & + \frac{2B_0 - h_1 \cot\alpha_{A1}}{2} h_1 \gamma_1 \\ & \left\{ \frac{(1 - k_v)\sin(\alpha_{A1} - \phi_1) + k_h \cos(\alpha_{A1} - \phi_1)}{\cos(\alpha_{A1} - \phi_1 - \delta_1)} \right\} - \\ & - \gamma_1 h_1 (B_0 - h_1 \cot\alpha_{A1}) \\ & \left\{ \frac{(1 - k_v)\sin(\alpha_{A1} - \phi_1) + k_h \tan\phi_2 \cos(\alpha_{A1} - \phi_1)}{\cos(\alpha_{A1} - \phi_1 - \delta_1)} \right\} - \\ & - 2c_1 h_1 \frac{\sin(\alpha_{A1} - \phi_1)}{\cos(\alpha_{A1} - \phi_1 - \delta_1)} - c_2 B_0 \frac{\cos(\alpha_{A1} - \phi_1)}{\cos(\alpha_{A1} - \phi_1 - \delta_1)} \\ & - c_1 h_1 \cot\alpha_{A1} \frac{\cos(\alpha_{A1} - \phi_1)}{\cos(\alpha_{A1} - \phi_1 - \delta_1)} + \\ & + c_2 h_1 \cot\alpha_{A1} \frac{\cos(\alpha_{A1} - \phi_1)}{\cos(\alpha_{A1} - \phi_1 - \delta_1)} \end{aligned} \tag{7}$$

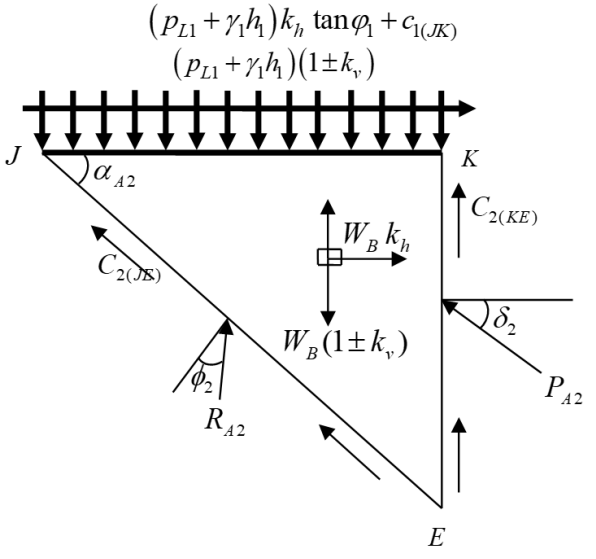

Figure 4: Active wedge in Bottom layer.

2.2 Active pressure at the bottom layer

From Fig. 4, active pressure distributing from the top layer tothe wedge *JKE*.

The weight of the wedge:

$$W_B = \frac{1}{2}(B_0 - h_1 \cot \alpha_{A1})\, h_2 \gamma_2 \tag{8}$$

Base shear at the interface between the two layers is given as:

$$\begin{aligned} &(p_{L1} + \gamma_1 h_1)\, k_h \ \tan \varphi_2 + c_2 \\ &\text{and} \\ &(p_{L1} + \gamma_1 h_1)\, k_h \ \tan \varphi_1 + c_1 \end{aligned} \tag{9}$$

Total cohesive force at the slip lines JE and KE is expressed as:

$$\begin{aligned} &C_{2(KE)} = c_2 KE = c_2 h_2, \\ &C_{2(JE)} = c_2 JE = c_2 h_2 \cos ec \alpha_{A2} \\ &\text{and} \\ &C_{1(JK)} = c_1 JK = c_1 (B_0 - h_1 \cot \alpha_{A1}) \end{aligned} \tag{10}$$

Conceding to limit equilibrium conditions,

$$\sum V = 0$$

$$\begin{aligned} &\Rightarrow C_{2(JE)} \sin \alpha_{A2} + C_{2(KE)} + \\ &+ R_{A2} \cos(\alpha_{A2} - \phi_2) + P_{A2} \sin \delta_2 - \\ &- (p_{L1} + \gamma_1 h_1) JK (1 - k_v) - W_B (1 - k_v) = 0 \end{aligned} \tag{11}$$

$$\sum H = 0$$

$$\begin{aligned} &\Rightarrow C_{1(JK)} - C_{2(JE)} \cos \alpha_{A2} + \\ &+ R_{A2} \sin(\alpha_{A2} - \phi_2) - P_{A2} \cos \delta_2 + \\ &+ (p_{L1} + \gamma_1 h_1) JK k_h \tan \phi_1 + W_B k_h = 0 \end{aligned} \tag{12}$$

Solving Equations 11 and 12 and simplifying them, we obtain

$$P_{A2} = f_1(p_{L1}, c_2, \phi_2, \gamma_2, \alpha_{A2}) \tag{13}$$

The details of equations of P_{A2} are given in **Appendix I.**

Hence, total active pressure from both the layers is given by

$$P_A = P_{A1} + P_{A2} \tag{14}$$

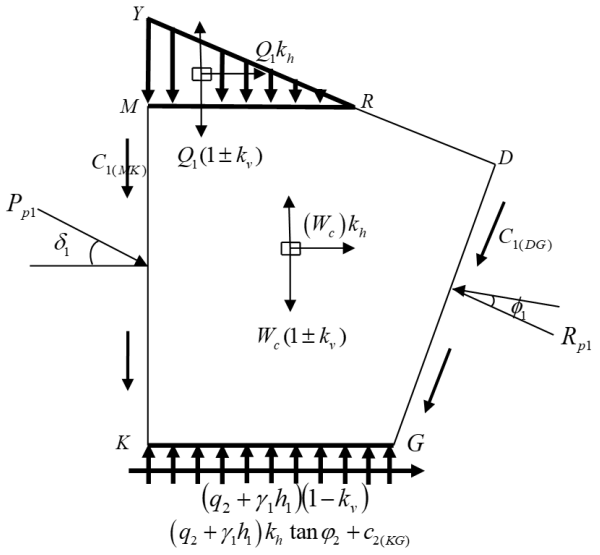

Figure 5: Passive wedge in Top layer.

2.3 Passive resistance at the top layer

Due to active pressure generated in the top layer, the passive zone gives resistance to the active pressure. The weight of the passive wedge, as depicted in Fig. 5, is given as

$$\begin{aligned} W_c = &\left[\frac{h_1 \cot \alpha_{p1} + 2h_2 \cot \alpha_{p2}}{2} h_1 - \right. \\ &\left. - \frac{1}{4}\left(h_1 \cot \alpha_{p1} + h_2 \cot \alpha_{p2} - \frac{D_f}{\tan i} + \frac{B_0}{2}\right)^2 \tan \alpha_{p1}\right] \gamma_1 \end{aligned} \tag{15}$$

Extra loadingacting on the foundation is expressed as surcharge load

$$\begin{aligned} q_1 &= \gamma_1 (YM/2) \\ &= \gamma_1 \frac{1}{2} \tan i \left(\frac{D_f}{\tan i} - \frac{B_0}{2}\right) \end{aligned} \tag{16}$$

Total surcharge load in the top layer of the passive zone is given as

$$\begin{aligned} Q_1 &= q_1 MR \\ &= \frac{\gamma_1}{2} \tan i \left(\frac{D_f}{\tan i} - \frac{B_0}{2}\right)^2 \end{aligned} \tag{17}$$

Total cohesive force in the slip lines KG and GD of the passive wedge is given as

$$\begin{aligned} &C_{1(KG)} = c_1 KG = c_1 h_2 \cot \alpha_{p2}, C_{1(MK)} = c_1 MK = c_1 h_1 \\ &C_{1(GD)} = c_1 GD = c_1 h_1 \cos ec \alpha_{p1} - \\ &- c_1 \left\{\frac{1}{2}\left(h_1 \cot \alpha_{p1} + h_2 \cot \alpha_{p2} - \frac{D_f}{\tan i} + \frac{B_0}{2}\right) \sec \alpha_{p1}\right\} \end{aligned} \tag{18}$$

Using limit equilibrium equations

$$\sum V = 0$$

$$\Rightarrow -C_{1(MK)} - C_{1(GD)} \sin \alpha_{p1} + \\ + R_{p1} \cos\left(\phi_1 + \alpha_{p1}\right) - P_{p1} \sin \delta_1 + \\ + (q_2 + \gamma_1 h_1) KG (1 - k_v) - \\ - (Q_1 + W_c)(1 - k_v) = 0 \tag{19}$$

$$\sum H = 0$$

$$\Rightarrow -C_{1(GD)} \cos \alpha_{p1} + C_{1(GK)} - \\ - R_{p1} \sin\left(\phi_1 + \alpha_{p1}\right) + P_{p1} \cos \delta_1 + \\ + (q_2 + \gamma_1 h_1) KG k_h \tan \phi_2 + \\ + (Q_1 + W_c) k_h = 0 \tag{20}$$

Solving Equations 19 and 20 and modifying both equations, passive resistance can be expressed as:

$$P_{p1} = [\frac{h_1 \cot \alpha_{p1} + h_2 \cot \alpha_{p2}}{2} h_1 - \\ - \frac{1}{4}\left(h_1 \cot \alpha_{p1} + h_2 \cot \alpha_{p2} - \frac{D_f}{\tan i} + \frac{B_0}{2}\right)^2 \tan \alpha_{p1}]\gamma_1 \\ \left\{\frac{(1 - k_v)\sin\left(\phi_1 + \alpha_{p1}\right) - k_h \cos\left(\phi_1 + \alpha_{p1}\right)}{\cos\left(\phi_1 + \alpha_{p1} + \delta_1\right)}\right\} \\ - \gamma_1 h_1 h_2 \cot \alpha_{p2} \left\{\frac{(1 - k_v)\sin\left(\phi_1 + \alpha_{p1}\right) + k_h \tan \phi_2 \cos\left(\phi_1 + \alpha_{p_1}\right)}{\cos\left(\phi_1 + \alpha_{p1} + \delta_1\right)}\right\} \\ - \gamma_1 \frac{\tan\left(\frac{D_f}{\tan i} - \frac{B_0}{2}\right)\left(2D_f - B_0 \tan i\right)}{2D_f + \tan i\,(2h_1 - B_0)} h_2 \cot \alpha_{p2} \\ \left\{\frac{(1 - k_v)\sin\left(\phi_1 + \alpha_{p1}\right) + k_h \tan \phi_2 \cos\left(\phi_1 + \alpha_{p1}\right)}{\cos\left(\phi_1 + \alpha_{p1} + \delta_1\right)}\right\} \\ + \gamma_1 \tan i \left(\frac{D_f}{\tan i} - \frac{B_0}{2}\right)^2 \left\{\frac{(1 - k_v)\sin\left(\phi_1 + \alpha_{p1}\right) - k_h \cos\left(\phi_1 + \alpha_{p1}\right)}{\cos\left(\phi_1 + \alpha_{p1} + \delta_1\right)}\right\} + \\ c_1 h_1 \left\{\frac{\sin\left(\phi_1 + \alpha_{p1}\right)}{\cos\left(\phi_1 + \alpha_{p1} + \delta_1\right)}\right\} \\ + c_1 \sin \alpha_{p1}\left[\frac{h_1}{2} \cos ec\alpha_{p1} - \frac{h_2}{2} \cot \alpha_{p2} \sec \alpha_{p1} + \frac{1}{2}\frac{D_f}{\tan i} \sec \alpha_{p1} - \frac{B_0}{4} \sec \alpha_{p1}\right] \\ \left\{\frac{\sin\left(\phi_1 + \alpha_{p1}\right)}{\cos\left(\phi_1 + \alpha_{p1} + \delta_1\right)}\right\} \\ + c_1 \cos \alpha_{p1}\left[\frac{h_1}{2} \cos ec\alpha_{p1} - \frac{h_2}{2} \cot \alpha_{p2} \sec \alpha_{p1} + \frac{1}{2}\frac{D_f}{\tan i} \sec \alpha_{p1} - \frac{B_0}{4} \sec \alpha_{p1}\right] \\ \frac{\cos\left(\phi_1 + \alpha_{p1}\right)}{\cos\left(\phi_1 + \alpha_{p1} + \delta_1\right)} - c_1 h_2 \cot \alpha_{p2} \frac{\cos\left(\phi_1 + \alpha_{p1}\right)}{\cos\left(\phi_1 + \alpha_{p1} + \delta_1\right)} \tag{21}$$

2.4 Passive resistance at the bottom layer

Total weight of the passive wedge KGE, as shownin Fig. 6, is calculated as

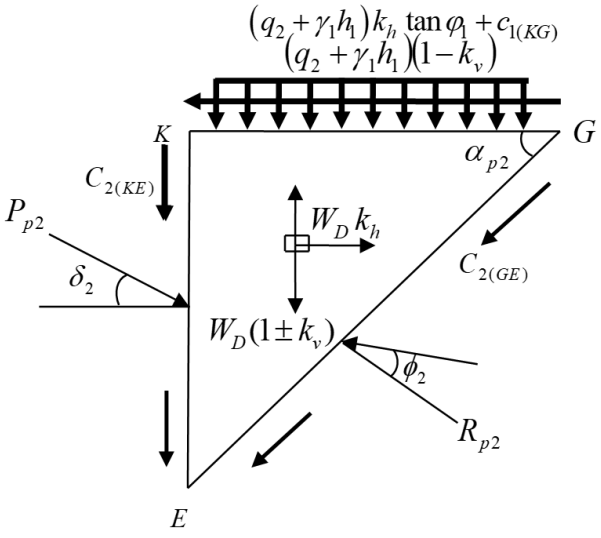

Figure 6: Passive wedge in Bottom layer.

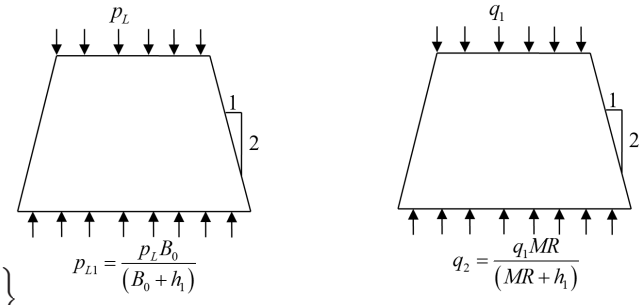

Figure 7: Load spread mechanism.

$$W_D = \frac{1}{2} {h_2}^2 \cot \alpha_{p2} \gamma_2 \tag{22}$$

According to 2 : 1 load distribution method, intensity of surcharge load at depth h_1 can be written as

$$q_2 = \frac{q_1 MR}{(MR + h_1)} \\ = \frac{\frac{\gamma_1}{2}\tan i \left(\frac{D}{\tan i} - \frac{B_0}{2}\right)^2}{\left(\frac{D_f}{\tan i} - \frac{B_0}{2}\right) + h_1} \tag{23}$$

Base shear between two passive wedges can be coded as

$$(q_2 + \gamma_1 h_1) k_h \tan \varphi_2 + c_1 \quad \text{and} \quad (q_2 + \gamma_1 h_1) k_h \tan \varphi_1 + c_1 \tag{24}$$

Cohesive forces in slip lines KE, KG and GE are given as

Case 1: Considering the effective area of active zones

$$\bar{\gamma} = \frac{\frac{\left(2-\frac{h_1}{B_0}\cot\alpha_{A1}\right)}{2}h_1\gamma_1 + \frac{\left(1-\frac{h_1}{B_0}\cot\alpha_{A1}\right)}{2}h_2\gamma_2}{\frac{\left(2-\frac{h_1}{B_0}\cot\alpha_{A1}\right)}{2}h_1 + \frac{\left(1-\frac{h_1}{B_0}\cot\alpha_{A1}\right)}{2}h_2} \tag{33}$$

Case 2: Considering the effective area of passive zones

$$\bar{\gamma} = \frac{\left\{\left(\frac{h_1}{B_0}\cot\alpha_{p1} + 2\frac{h_2}{B_0}\cot\alpha_{p2}\right)\frac{h_1}{2B_0} - \frac{1}{4}\left(\frac{h_1}{B_0}\cot\alpha_{p1} + \frac{h_2}{B_0}\cot\alpha_{p2} - \frac{D_f}{B_0\tan i} + \frac{1}{2}\right)^2\tan\alpha_1\right\}\gamma_1 + \frac{1}{2}\left(\frac{h_2}{B_0}\right)^2\cot\alpha_{p2}\gamma_2}{\left\{\left(\frac{h_1}{B_0}\cot\alpha_{p_1} + 2\frac{h_2}{B_0}\cot\alpha_{p2}\right)\frac{h_1}{2B_0} - \frac{1}{4}\left(\frac{h_1}{B_0}\cot\alpha_{p1} + \frac{h_2}{B_0}\cot\alpha_{p2} - \frac{D_f}{B_0\tan i} + \frac{1}{2}\right)^2\tan\alpha_1\right\} + \frac{1}{2}\left(\frac{h_2}{B_0}\right)^2\cot\alpha_{p2}} \tag{34}$$

The bearing capacity factor $(N_{\gamma'})$ is a function of several parameters including cohesion, surcharge and unit weight. It can be expressed as:

$$N_{\gamma''} = \left(\frac{a_1}{e_1} + \frac{b_1}{e_1} + \frac{2\bar{c}}{\bar{\gamma}B_0}\frac{d_1}{e_1}\right) \tag{35}$$

The details of the equations a_1, b_1, e_1 and $d_1$are given in **Appendix II.**

Where $\bar{c}$ is averaged cohesion in each layer in the slip line is shown by

$$\bar{c} = \frac{c_1h_1 + c_2h_2}{h_1 + h_2} \tag{36}$$

a_1, b_1, e_1 and d_1 are dimensionless equations.

In seismic condition, $(N_{\gamma''})$ can be expressed as $(N_{\gamma E})$ and in static condition, $(N_{\gamma''})$ can be expressed as $(N_{\gamma S})$, whereas $(N_{\gamma''})$ is the unity factor for the simultaneous resistance of unit weight, surcharge and cohesion.

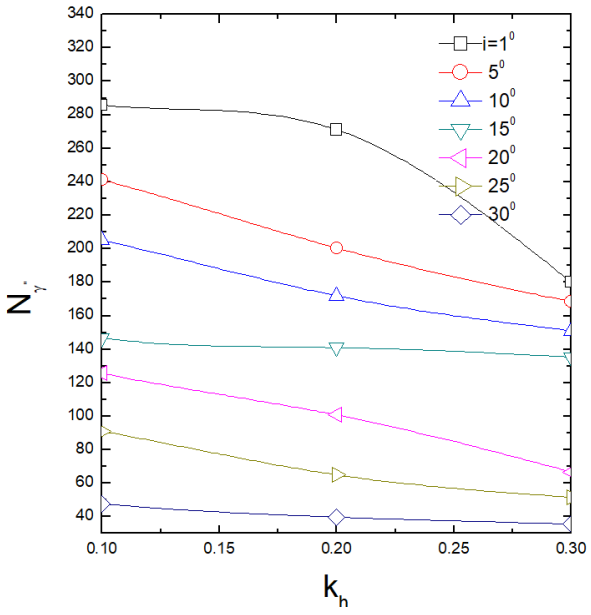

Figure 8: Design chart of Bearing capacity coefficient at $\phi_2 = 30°, \delta_2 = \phi_2/2, i = 15^0, \delta_1/\delta_2 = 0.8, k_v = k_h/2, \gamma_1/\gamma_2 = 0.8, D_f/B_0 = 0.5, h_1/B_0 = 0.25, 2c_2/B_0\gamma_2 = 0.2, c_1/c_2 = 0.8.$

3 Results and Discussion

The bearing capacity factor $(N_{\gamma''})$ has been computed by PSO algorithm, with the optimum $(N_{\gamma''})$ optimized w.r.t. variables α_{A1}, α_{A2}, α_{p1} and α_{p2}. The minimum value is taken as an optimised value. The design charts of the obtained bearing capacity coefficients $(N_{\gamma''})$ for different values of slope angle (i) are shown in Figs 8 and 9 ($\phi = 30°, 40°$, $\frac{D_f}{B_0} = 1$). It has been observed that $(N_{\gamma''})$ decreases when the slope angle (i) increases. The results obtained from MATLAB are summarised in design Tables 1 and 2. Using these design tables, the bearing capacity coefficients of the strip footing near slope are easily obtained with sufficient accuracy from the engineering point of view.Undrained bearing capacity is expressed as N_{cs} in the design tables.

3.1 Computation of N_{cs}

Merifield et al. (1999) investigated the bearing capacity of a strip footing resting on a two-layer clay deposit with a horizontal ground surface and proposed a modified bearing capacity factor N_c^*, which can be expressed as:

$$N_c^* = \frac{q_u}{c_1} \tag{37}$$

where $q_{u=}$ ultimate bearing capacity and c_1= undrained shear strength of the top layer.

Similarly, a dimensionless undrained bearing capacity factor N_{cs} is defined in the present study, which is a function of the parameters $c_u/\gamma B_0$, D_f/B_0, $c_1/c_2, i, k_h$ and it can be described by the following equation:

$$N_{cs} = q_{ult}/c_1 = f\left(c_u/\gamma B_0, D_f/B_0, c_1/c_2, i, k_h\right) \tag{38}$$

Table 1: Undrained seismic bearing capacity N_{cs} for strip footing placed adjacent to two layered slope with i=15°.

k_h	D_f/B_0	c_1/c_2	$c_1/\gamma B_0$				k_h	D_f/B_0	c_1/c_2	$c_1/\gamma B_0$			
			1	2	4	6				1	2	4	6
		0.25	5.52	5.54	5.56	5.56			0.25	4.54	4.60	4.62	4.64
		0.5	5.52	5.54	5.56	5.56			0.5	4.52	4.60	4.61	4.63
		0.75	5.42	5.37	5.43	5.46			0.75	4.52	4.60	4.60	4.62
		1	4.74	4.40	4.41	4.42			1	4.36	4.42	4.44	4.47
	0.25	1.5	3.05	3.17	3.22	3.22		0.50	1.5	3.32	3.45	3.52	3.54
		2	2.4	2.52	2.58	2.6			2	1.55	2.82	2.90	2.92
		3	-	1.80	1.85	1.88			3	–	2.12	2.22	2.24
		4	-	0.6	1.51	1.53			4	–	0.91	1.84	1.90
		5	-	–	1.29	1.31			5	–	–	1.61	1.64
		0.25	4.50	4.46	4.25	4.49			0.25	4.40	4.49	4.52	4.53
		0.5	4.5	4.48	4.53	4.59			0.5	4.39	4.49	4.52	4.53
		0.75	4.4	4.4	4.54	4.58			0.75	4.38	4.49	4.52	4.53
		1	4.35	4.2	4.45	4.49			1	4.38	4.44	4.47	4.48
0	0.75	1.5	4.05	3.84	3.93	3.96	0	1	1.5	3.88	4.2	4.3	4.33
		2	3.45	3.24	3.36	3.4			2	1.87	3.62	3.76	3.82
		3	-	2.44	2.62	2.68			3	–	2.7	3.07	3.13
		4	-	1.12	2.20	2.28			4	–	1.38	2.64	2.71
		5	-	–	1.92	2.0			5	–	–	2.27	2.42
		0.25	4.42	4.46	4.50	4.52			0.25	4.44	4.50	4.52	4.53
		0.5	4.41	4.43	4.48	4.51			0.5	4.41	4.49	4.52	4.53
		0.75	4.40	4.42	4.47	4.50			0.75	4.41	4.49	4.52	4.54
		1	4.39	4.41	4.45	4.48			1	4.38	4.44	4.47	4.48
	1.25	1.5	4.01	3.59	3.74	3.85		1.5	1.5	4.17	4.49	4.52	4.44
		2	3.67	3.2	3.42	3.45			2	2.34	4.18	4.31	4.37
		3	-	2.64	2.92	2.97			3	–	3.1	3.54	3.74
		4	-	1.67	2.59	2.67			4	–	1.92	3.3	3.43
		5	-	–	2.36	2.48			5	–	–	2.87	3.12
		0.25	4.84	4.79	4.8	4.81			0.25	4.12	4.2	4.23	4.24
		0.5	4.82	4.78	4.8	4.81			0.5	4.13	4.2	4.24	4.24
		0.75	4.64	4.79	4.8	4.81			0.75	4.13	4.2	4.24	4.24
		1	4.12	4.15	4.2	4.21			1	4.06	4.15	4.19	4.21
	0.25	1.5	-	3.03	3.09	3.11		0.5	1.5	–	3.37	3.46	3.5
		2	-	2.42	2.49	2.51			2	–	2.76	2.87	2.91
		3	-	–	1.82	1.87			3	–	–	2.21	2.25
		4	-	–	1.47	1.51			4	–	–	1.85	1.89
		5	-	–	–	1.28			5	–	–	–	1.65
		0.25	4.11	4.14	4.18	4.2			0.25	4.06	4.15	4.18	4.19
		0.5	4.08	4.13	4.18	4.19			0.5	4.05	4.14	4.19	4.19
		0.75	4.06	4.14	4.18	4.19			0.75	4.04	4.13	4.18	4.19
		1	4.04	4.15	4.2	4.21			1	4.02	4.11	4.14	4.17
0.1	0.75	1.5	-	3.74	3.85	3.89	0.1	1	1.5	–	4.07	4.18	4.2
		2	-	3.13	3.31	3.36			2	–	3.48	3.71	3.79
		3	-	–	2.61	2.68			3	–	–	3.01	3.1
		4	-	–	2.14	2.28			4	–	–	2.34	2.67
		5	-	–	–	2.02			5	–	–	–	2.38
		0.25	4.08	4.14	4.18	4.19			0.25	4.05	4.14	4.18	4.19
		0.5	4.06	4.14	4.18	4.2			0.5	4.04	4.14	4.18	4.19
		0.75	4.05	4.13	4.18	4.19			0.75	4.05	4.14	4.18	4.19
		1	4.04	4.15	4.2	4.21			1	4.06	4.14	4.19	4.2
	1.25	1.5	-	4.14	4.19	4.2		1.5	1.5	–	4.14	4.19	4.2
		2	-	3.84	4.07	4.16			2	–	3.95	4.18	4.2
		3	-	–	3.37	3.48			3	–	–	3.67	3.82
		4	-	–	2.54	3.05			4	–	–	2.72	3.38
		5	-	–	–	2.68			5	–	–	–	2.98

Table 2: Undrained seismic bearing capacity N_{cs} for strip footing placed adjacent to two layered slope with i=30°.

k_h	D_f/B_0	c_1/c_2	$c_1/\gamma B_0$				k_h	D_f/B_0	c_1/c_2	$c_1/\gamma B_0$			
			1	2	4	6				1	2	4	6
		0.25	5.12	5.16	5.18	5.19			0.25	4.06	4.14	4.21	4.23
		0.5	5.12	5.16	5.18	5.19			0.5	4.05	4.13	4.19	4.22
		0.75	4.82	4.91	4.96	4.97			0.75	4.03	4.11	4.17	4.20
		1	3.8	3.96	4.03	4.05			1	3.8	3.96	4.06	4.08
	0.25	1.5	2.23	2.81	2.9	2.93		0.5	1.5	2.32	3.01	3.10	3.12
		2	–	2.18	2.3	2.33			2	–	2.45	2.61	2.65
		3	–	1.25	1.68	1.72			3	–	1.44	2	2.06
		4	–	–	1.33	1.38			4	–	–	1.65	1.72
		5	–	–	1	1.17			5	–	–	1.24	1.5
		0.25	3.82	3.97	4.06	4.09			0.25	3.80	3.92	4.04	4.06
		0.5	3.83	3.97	4.06	4.09			0.5	3.80	3.92	4.04	4.06
		0.75	3.82	3.97	4.07	4.09			0.75	3.80	3.91	4.04	4.06
		1	3.8	3.96	4.06	4.09			1	3.82	3.96	4.03	4.05
0	0.75	1.5	2.51	3.25	3.37	3.41	0	1	1.5	2.64	3.44	3.59	3.64
		2	–	2.73	2.9	2.95			2	–	2.96	3.17	3.23
		3	–	1.67	2.31	2.38			3	–	1.86	2.56	2.67
		4	–	–	1.92	2.05			4	–	–	2.17	2.34
		5	–	–	1.5	1.8			5	–	–	1.74	2.07
		0.25	3.83	3.96	4.03	4.06			0.25	3.8	3.96	4.03	4.05
		0.5	3.83	3.96	4.03	4.05			0.5	3.79	3.96	4.02	4.04
		0.75	3.83	3.96	4.03	4.05			0.75	3.8	3.96	4.03	4.05
		1	3.83	3.96	4.03	4.05			1	3.8	3.96	4.03	4.05
	1.25	1.5	2.74	3.65	3.84	3.9		1.5	1.5	2.8	3.84	4.01	4.04
		2	–	3.2	3.45	3.53			2	–	3.41	3.71	3.8
		3	–	2.1	2.9	3.02			3	–	2.33	3.18	3.32
		4	–	–	2.43	2.64			4	–	–	2.69	2.94
		5	–	–	2.02	2.35			5	–	–	2.28	2.64
		0.25	4.25	4.31	4.34	4.34			0.25	3.57	3.68	3.74	3.76
		0.5	4.25	4.31	4.34	4.35			0.5	3.57	3.69	3.74	3.76
		0.75	4.25	4.31	4.33	4.33			0.75	3.57	3.69	3.74	3.76
		1	3.44	3.6	3.67	3.7			1	3.44	3.61	3.68	3.71
	0.25	1.5	–	2.6	2.7	2.73		0.5	1.5	–	2.82	2.94	2.97
		2	–	2.03	2.15	2.19			2	–	2.29	2.46	2.5
		3	–	–	1.57	1.61			3	–	–	1.89	1.95
		4	–	–	1.23	1.3			4	–	–	1.48	1.64
		5	–	–	–	1.1			5	–	–	–	1.4
		0.25	3.45	3.61	3.68	3.7			0.25	3.44	3.61	3.68	3.7
		0.5	3.45	3.61	3.68	3.7			0.5	3.44	3.61	3.68	3.7
		0.75	3.45	3.61	3.68	3.7			0.75	3.45	3.61	3.68	3.71
		1	3.45	3.61	3.68	3.7			1	3.45	3.61	3.68	3.7
0.1	0.75	1.5	–	3.04	3.18	3.22	0.1	1	1.5	–	3.23	3.44	3.5
		2	–	2.55	2.75	2.81			2	–	2.78	3.04	3.12
		3	–	–	2.2	2.28			3	–	–	2.5	2.62
		4	–	–	1.74	1.96			4	–	–	2.03	2.27
		5	–	–	–	1.74			5	–	–	–	1.97
		0.25	3.45	3.61	3.68	3.67			0.25	3.44	3.61	3.68	3.7
		0.5	3.44	3.61	3.68	3.67			0.5	3.44	3.61	3.68	3.7
		0.75	3.44	3.61	3.68	3.67			0.75	3.44	3.61	3.68	3.7
		1	3.45	3.61	3.68	3.7			1	3.45	3.62	3.68	3.7
	1.25	1.5	–	3.47	3.68	3.71		1.5	1.5	–	3.61	3.68	3.7
		2	–	2.95	3.3	3.38			2	–	3.13	3.59	3.68
		3	–	–	2.76	2.91			3	–	–	3.06	3.24
		4	–	–	2.18	2.54			4	–	–	2.33	2.86
		5	–	–	–	2.22			5	–	–	–	2.53

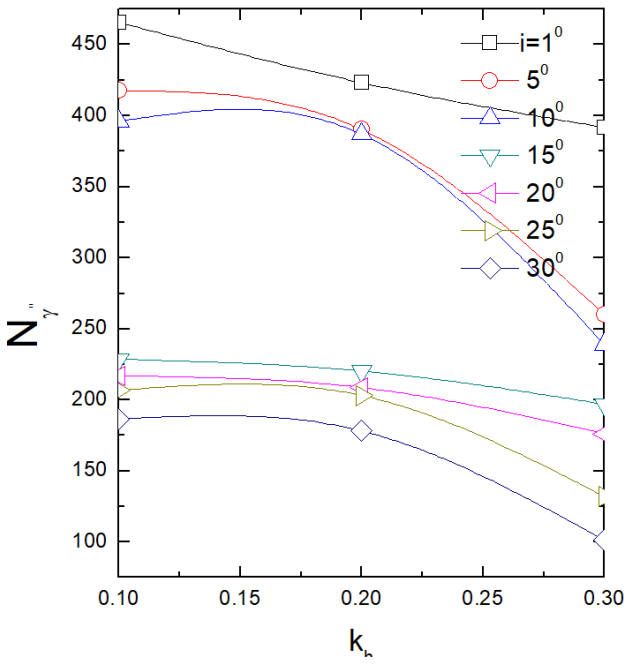

Figure 9: Design chart of Bearing capacity coefficient at $\phi_2 = 40°, \delta_2 = \phi_2/2, i = 15^0, \delta_1/\delta_2 = 0.8, k_v = k_h/2, \gamma_1/\gamma_2 = 0.8, D_f/B_0 = 1, h_1/B_0 = 0.25, 2c_2/B_0\gamma_2 = 0.2, c_1/c_2 = 0.8$

Ranges of various parameters are given as follows:

$\frac{\phi_1}{\phi_2} = 0.6, 0.8, 1\ \frac{\gamma_1}{\gamma_2} = 0.6, 0.8, 1\ \frac{h_1}{B_0} = 0.1, 0.25, 0.5$

$$i = 10^0, 15^0, 20^0, 25^0 k_v = 0,\ k_h/2,\ k_h$$

$\frac{\delta_1}{\delta_2}$ is the ratio of wall friction angles between the top and bottom layers.

Since the heuristic algorithms give us low ramification and high execution and these methods are relatively new, they can be applied in the geotechnical problem. Out of these methods, a brief discussion on PSO is given here as it is used in the analysis.

3.2 Particle swarm optimisation

Kennedy and Eberhart (1995) developed PSO as a simulation of birds swarm. A swarm is a group of individuals with defined rules for individual behaviours and communication. The ability of each individual to deal with the previous experiences of the swarm is called swarm intelligence. This capability guides the swarm towards its optimum goal. PSO is a population-based search technique where a population of particles start their journey in a space concerning the current best position (Hossain and EI-Shafie 2014; Hajihassani et al.2017). Reynolds (1987) described three simple rules for the behaviours of individuals inside a swarm, which were used as one of the basic concepts of PSO by Kennedy and Eberhart (1995). Although these simple rules model the behaviour of individuals, their combination produces a complicated behaviour for the swarm.

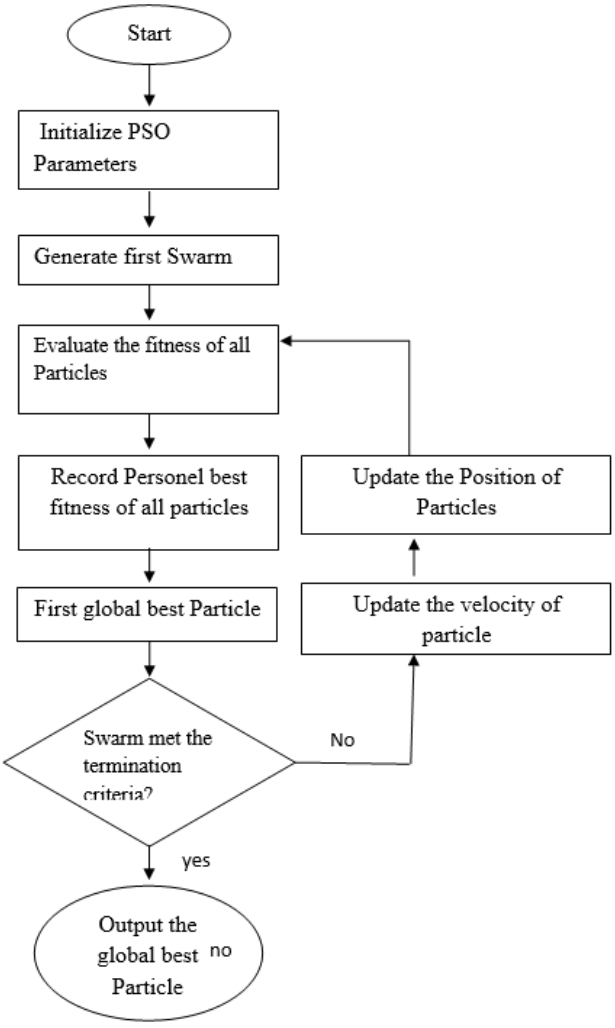

Figure 10: Flowchart of PSO algorithm.

1. Individuals avoid collision with others
2. Individuals go towards the goal of the swarm
3. Individuals go to the centre of the swarm

The process of decision-making related to individuals is another basic concept of PSO. Each individual of the swarm makes decisionbased on the following two factors:

1. Own experiences of the individual that is its bestresults so far
2. The experiences of other individuals in the swarm that is the best results in the whole swarm

Figure 10 illustrates the standard flowchart of PSO. At the starting step of the original PSO, a certain num-

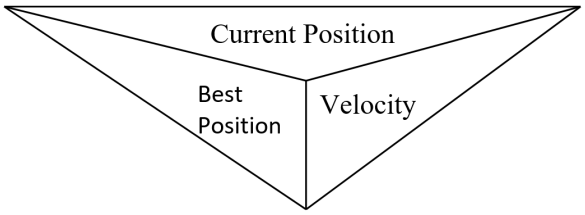

Figure 11: Schematic structure of a particle in PSO (Kalatehjari 2013).

ber of individuals, called particles, are distributed in the search space by using a random pattern (Kennedy and Eberhart 1995; Cheng et al. 2007; Aote et al. 2013). Each particle is representative of a feasible solution. Figure 11 shows the schematic structure of a particle in PSO involving three divided parts as its current position, best position and velocity. The current position, best position and velocity of particles record the current coordinates, best coordinates and velocity vectors of a particle in D-dimensional space,respectively, where D starts from 1 (Kalatehjari 2013). Consequently, for a particle in D-dimensional space, a 3D-dimensional particle is desirable. PSO aims to meet the termination criteria which are defined as the criteria for terminating the iterative search process. To select an appropriate termination criterion, it should be noted that the termination condition does not cause a premature converge and it should protect against oversampling of the fitness (Engelbrecht 2007). The following termination criteria are frequently used in PSO:

1. Termination when the maximum number ofiterations is exceeded
2. Termination when a satisfactory solution isfound based on the condition of each problem
3. Termination when no improvement is achievedover a certain number of iterations

These criteria are applied to ensure that PSO can converge on a feasible solution. Although PSO has some limitation which is explained by Gbenga et al. (2016) and Aote et al. (2013), PSO tries to make the objective function as a minimum or maximum dependingon the problem to be solved. To lead the swarm towards this aim, the fitness value of each particle is determined by evaluating its current position by the objective function. After evaluation offitness of all particles, Equation 39 (velocity equation) is used to calculate the velocity of particles based on their best position and the position of the best particle in the swarm.Using Equation 40, particle positions can be updated according to their current positions and velocities. This iterative process continues until reaching the termination criteria. Equations 39 and 40 are as follows (Kennedy and Eberhart 1995):

$$v_{n(i)} = v_{n(i-1)} + u\,(0, \vartheta_1)\left(b_{p_{n(i)}} - X_{n(i)}\right) + \\ + u\,(0, \vartheta_2)\left(b_{g_{n(i)}} - X_{n(i)}\right) \tag{39}$$

$$X_{n(i+1)} = X_{n(i)} + v_{n(i)} \tag{40}$$

where v is the velocity of an nth particle in the past iteration and $v_{(n-1)}$ is the velocity of the nth particle in the current iteration. The vectors of random numbers ofan n^{th} particle are presented by $u(0, \vartheta_1)$ and $u(0, \vartheta_2)$, $b_{p_{n(i)}}$ is the best position of the nth particle so far, $b_{g_{n(i)}}$ is the position of the best particle of the swarm so far, and $X_{n(i-1)}$ and $X_{n(i)}$ are the positions of the nth particle in the current and next iterations,respectively. Input parameters are taken for optimisation as follows:

$$\text{Input } h_1/B_0, \phi_2, \phi_1/\phi_2, \delta_2, \delta_1/\delta_2, 2\bar{c}/\bar{\gamma}B_0,$$
$$k_h, k_v, \xi, \alpha_{A1} = 20^0 - 80^0 \alpha_{A2} = 30^0 - 80^\circ$$
$$\alpha_{p1} = 30^0 - 80^0 \alpha_{p2} = 30^0 - 60^0$$

3.3 Parametric study

3.3.1 Weak soil layer over strong soil layer

Aparametric study was done for the variation of pseudostatic seismic bearing capacity coefficients with different soil parameters as shown in Figs 12–18.

3.3.2 Variations of seismic bearing capacity coefficient for different values of slope angle (*i*) using PSO algorithm

Figure 12 shows the variation of seismic bearing capacity coefficient $\left(N_{\gamma E}\right)$ at $\phi_2 = 30^0$, $\delta_2 = \frac{\phi_2}{2}$, $\frac{\phi_1}{\phi_2} = 0.8$, $\frac{\delta_1}{\delta_2} = 0.8, k_v = \frac{k_h}{2}$, $\frac{\gamma_1}{\gamma_2} = 0.8, \frac{D_f}{B_0} = 0.5$, $\frac{h_1}{B_0} = 0.5$, $\frac{2c_2}{\gamma_2 B_0} = 0.2$ and $\frac{c_1}{c_2} = 0.8$ with k_h. From the plot, it is seen that $N_{\gamma E}$ decreases with the increase of angle of inclination (i). As the slope angle is increased, the area of the slope is decreased; therefore, the failure zone is decreased, resulting in much smaller bearing capacity.

3.3.3 Variations of seismic bearing capacity coefficient for different values of $\frac{\phi_1}{\phi_2}$ using PSO algorithm

Figure 13 depicts the variations of seismic bearing capacity coefficient $\left(N_{\gamma E}\right)$ at $\phi_2 = 30^0$, $\delta_2 = \frac{\phi_2}{2}$, $i = 15^0$, $\frac{\delta_1}{\delta_2} = 0.8$,

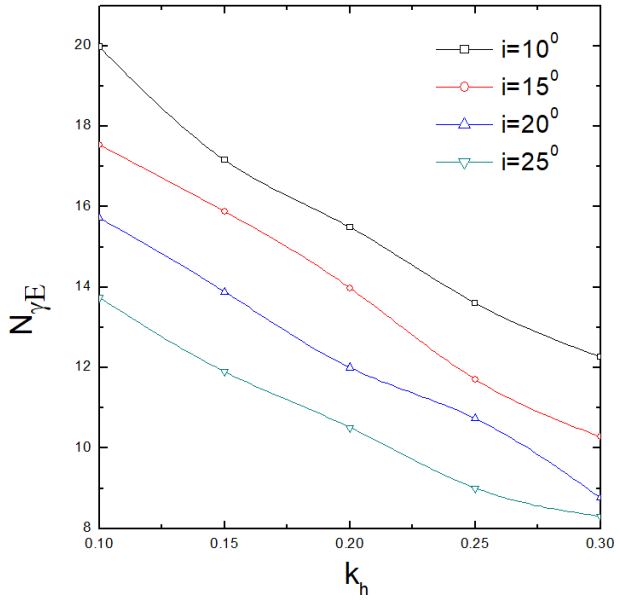

Figure 12: Variation of $N_{\gamma E}$ with k_h for $\phi_2 = 30°$, $\delta_2 = \phi_2/2$, $\phi_1/\phi_2 = 0.8$, $\delta_1/\delta_2 = 0.8$, $k_v = k_h/2$, $\gamma_1/\gamma_2 = 0.8$, $D_f/B_0 = 0.5$, $h_1/B_0 = 0.25$, $2c_2/B_0\gamma_2 = 0.2$, $c_1/c_2 = 0.8$.

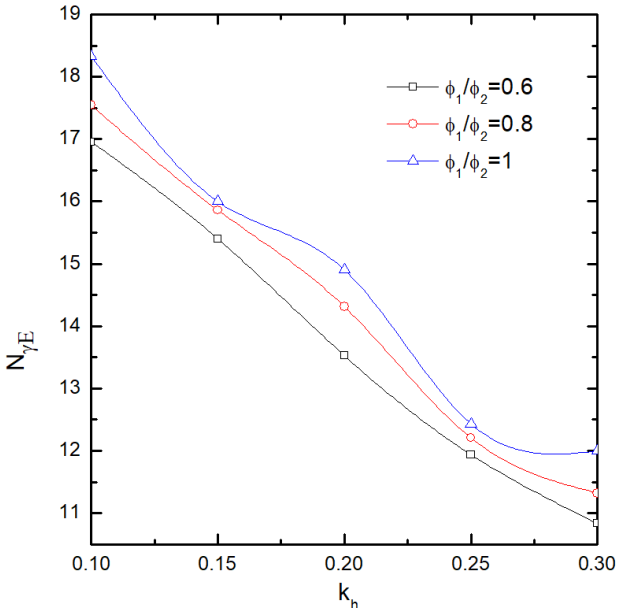

Figure 13: Variation of $N_{\gamma E}$ with k_h for $\phi_2 = 30°$, $\delta_2 = \phi_2/2$, $i = 15^0$, $\delta_1/\delta_2 = 0.8$, $k_v = k_h/2$, $\gamma_1/\gamma_2 = 0.8$, $D_f/B_0 = 0.5$, $h_1/B_0 = 0.25$, $2c_2/B_0\gamma_2 = 0.2$, $c_1c_2 = 0.8$.

$k_v = \frac{k_h}{2}$, $\frac{\gamma_1}{\gamma_2} = 0.8$, $\frac{D_f}{B_0} = 0.5$, $\frac{D_f}{B_0} = 0.5$, $\frac{2c_2}{\gamma_2 B_0} = 0.2$ and $\frac{c_1}{c_2} = 0.80$ with k_h. From the plot, it is seen that $N_{\gamma E}$ increases with an increase in the value of $\frac{\phi_1}{\phi_2}$. An increase in $\frac{\phi_1}{\phi_2}$ ratio increases the strength of the soil (or internal resistance of the soil) against the shearing resistance, which results in increasing the bearing capacity. Here, ϕ_1 value is increased while keeping the ϕ_2 value constant.

3.3.4 Variations of seismic bearing capacity coefficient for different values of $\frac{\gamma_1}{\gamma_2}$ using PSO algorithm

Figure 14 shows the variations of seismic bearing capacity coefficient $(N_{\gamma E})$ at $\phi_2 = 30^0$, $\delta_2 = \frac{\phi_2}{2}$, $i = 15^0$, $\frac{\delta_1}{\delta_2} = 0.8$,$k_v = \frac{k_h}{2}$, $\frac{\phi_1}{\phi_2} = 0.8$,$\frac{h_1}{B_0} = 0.25$, $\frac{D_f}{B_0} = 0.5$,$\frac{2c_2}{\gamma_2 B_0} = 0$ and $\frac{c_1}{c_2} = 0$ with k_h. From the plot, it is seen that coefficient $N_{\gamma E}$ increases with an increase in the value of $\frac{\gamma_1}{\gamma_2}$. Here, the ratio $\frac{\gamma_1}{\gamma_2}$ is increased while keeping γ_2 as a constant.

3.3.5 Variations of seismic bearing capacity coefficient for different values of $\frac{h_1}{B_0}$ using PSO algorithm

Figure 15 shows the variations of seismic bearing capacity coefficient $(N_{\gamma E})$ at $\phi_2 = 30^0$, $\delta_2 = \frac{\phi_2}{2}$,$i = 15^0$, $\frac{\delta_1}{\delta_2} = 0.8$,$k_v = \frac{k_h}{2}$, $\frac{\phi_1}{\phi_2} = 0.8$, $\frac{\gamma_1}{\gamma_2} = 0.80$, $\frac{D_f}{B_0} = 0.5$, $\frac{2c_2}{\gamma_2 B_0} = 0.2$ and $\frac{c_1}{c_2} = 0.8$ with k_h. From the plot, it is seen that $N_{\gamma E}$ decreases with an increase in the value of $\frac{h_1}{B_0}$. h_1 is the depth of the top layer and it is considered in the analysis that it is weaker than the bottom layer. So, a weaker layer will provide less resistance, and hence increase in the thickness of this layer decreases the value of bearing capacity coefficients.

3.3.6 Variations of seismic bearing capacity coefficient for different values of $\frac{\delta_1}{\delta_2}$ using PSO algorithm

Figure 16 shows the variation of seismic bearing capacity coefficient $(N_{\gamma E})$ at $\phi_2 = 30^0$, $\delta_2 = \frac{\phi_2}{2}$, $i = 15^0$, $\frac{h_1}{B_0} = 0.25$, $k_v = \frac{k_h}{2}$, $\frac{\phi_1}{\phi_2} = 0.8$, $\frac{\gamma_1}{\gamma_2} = 0.80$, $\frac{D_f}{B_0} = 0.5$, $\frac{2c_2}{\gamma_2 B_0} = 0.2$ and $\frac{c_1}{c_2} = 0.8$ with k_h. From the plot, it is seen that coefficient $N_{\gamma E}$ increases with an increase in the value of $\frac{\delta_1}{\delta_2}$.

3.3.7 Variations of seismic bearing capacity coefficient for different values of k_v using PSO algorithm

Figure 17 shows the variation of $N_{\gamma E}$ at $\phi_2 = 30^0$, $\delta_2 = \frac{\phi_2}{2}$, $i = 15^0$, $\frac{h_1}{B_0} = 0.25$, $\frac{c_1}{c_2} = 0.80$, $\frac{\phi_1}{\phi_2} = 0.8$, $\frac{\gamma_1}{\gamma_2} = 0.80$, $\frac{D_f}{B_0} = 0.5$, $\frac{2c_2}{\gamma_2 B_0} = 0.2$ and $\frac{\delta_1}{\delta_2} = 0.8$ with k_h. From the plot, it is seen that $N_{\gamma E}$ decreases with an increase in k_v. It is obvious because increase in the value of k_v increases the disturbance of base soil and this decreases the value of $N_{\gamma E}$.

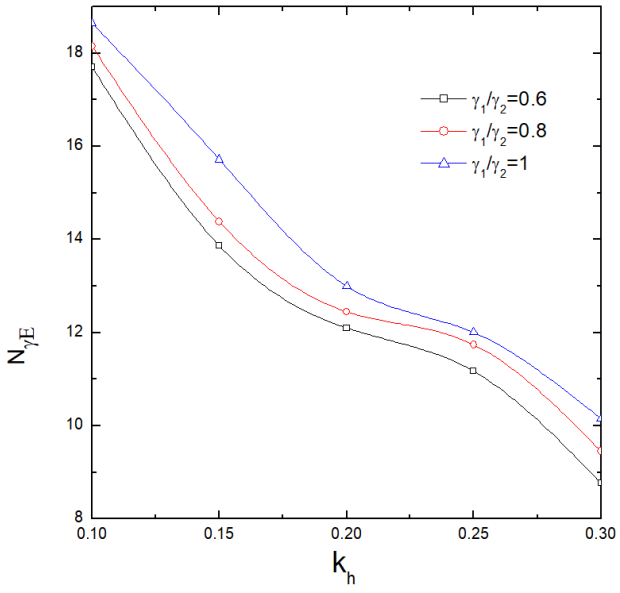

Figure 14: Variation of $N_{\gamma E}$ with k_h for $\phi_2 = 30^0$, $\delta_2 = \phi_2/2$, $i = 15^0$, $\delta_1/\delta_2 = 0.8$, $k_V = k_h/2$, $\phi_1/\phi_2 = 0.8$, $D_f/B_0 = 0.5$, $h_1/B_0 = 0.25$, $2c_2/B_0\gamma_2 = 0.2$, $c_1/c_2 = 0.8$.

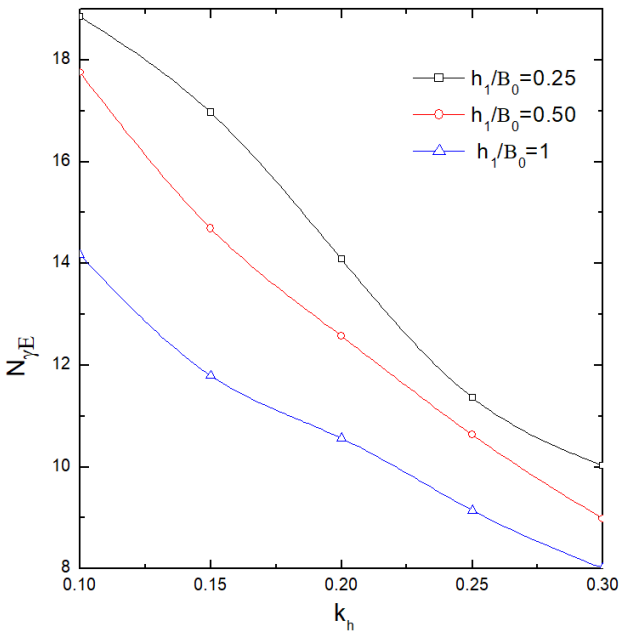

Figure 15: Variation of $N_{\gamma E}$ with k_h for $\phi_2 = 30°$, $\delta_2 = \phi_2/2$, $i = 15$, $\delta_1/\delta_2 = 0.8$, $k_v = k_h/2$, $\phi_1/\phi_2 = 0.8$, $D_f/B_0 = 0.5$, $\gamma_1/\gamma_2 = 0.80$, $2c_2/B_0\gamma_2 = 0.2$, $c_1/c_2 = 0.8$.

3.3.8 Variations of seismic bearing capacity coefficient for different values of $\frac{c_1}{c_2}$ using PSO algorithm

Figure 18 shows the variation of $N_{\gamma E}$at$\phi_2 = 30^0$, $\delta_2 = \frac{\phi_2}{2}$, $i = 15^0$, $\frac{h_1}{B_0} = 0.25$,$k_v = \frac{k_h}{2}$, $\frac{\phi_1}{\phi_2} = 0.8$, $\frac{\gamma_1}{\gamma_2} = 0.80$, $\frac{D_f}{B_0} = 0.5$, $\frac{2c_2}{\gamma_2 B_0} = 0.2$ and $\frac{\delta_1}{\delta_2} = 0.8$ with k_h. From the plot, it is seen that the coefficient $N_{\gamma E}$ increases with an increase in the value of $\frac{c_1}{c_2}$. By increasing the $\frac{c_1}{c_2}$ ratio, intermolecular attraction among the soil particles increases, which results in an increase in the bearing capacity.

3.3.9 Strong soil layer over weak soil layer

3.3.10 Variations of seismic bearing capacity coefficient for different values of using $\frac{\phi_1}{\phi_2}$ PSO algorithm

Figure 19 depicts the variations of seismic bearing capacity coefficient $(N_{\gamma E})$ at $\phi_2 = 20^0$, $\delta_2 = \frac{\phi_2}{2}$, $\frac{h_1}{B_0} = 0.25$, $\frac{\delta_1}{\delta_2} = 1.1$, $k_v = \frac{k_h}{2}$, $\frac{\gamma_1}{\gamma_2} = 1.1$, $\frac{D_f}{B_0} = 0.5$, $\frac{2c_2}{\gamma_2 B_0} = 0$ and $\frac{c_1}{c_2} = 0$ with k_h. From the figure, it is seen that the coefficient $N_{\gamma E}$ increases with an increase in the value of $\frac{\phi_1}{\phi_2}$. As the upper layer is considered a strong layer for this parameter, increasing the internal soil friction bearing capacity will be increased. Here, the ϕ_1 value is increased, keeping the ϕ_2 value constant.

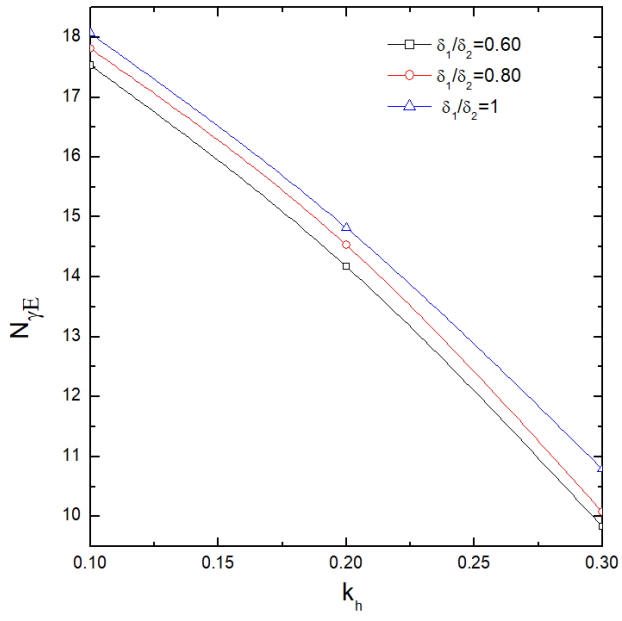

Figure 16: Variation of $N_{\gamma E}$ with k_h for $\phi_2 = 30°$, $\delta_2 = \phi_2/2$ $i = 15^0$, $c_2/c_2 = 0.8$, $k_V = k_h/2$, $\phi_1/\phi_2 = 0.8$, $D_f/B_0 = 0.5$, $h_1/B_0 = 0.25$, $\gamma_1/\gamma_2 = 0.8$.

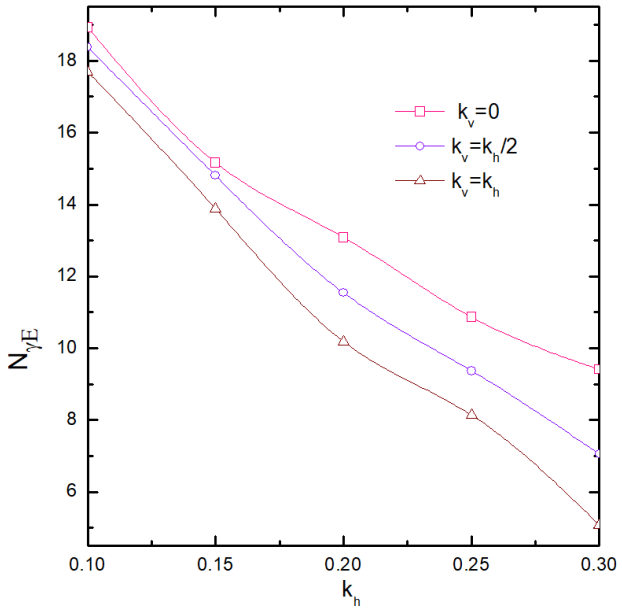

Figure 17: Variation of $N_{\gamma E}$ with k_h for $\phi_2 = 30$, $\delta_2 = \phi_2/2$, $D_f/B_0 = 0.5$ i = 20°, $h_1/B_0 = 0.25$, $\gamma_1/\gamma_2 = 0.8$, $\delta_1/\delta_2 = 0.8$, $\phi_1/\phi_2 = 0.8$, $2c_2/B_0\gamma_2 = 0$, $c_1/c_2 = 0$.

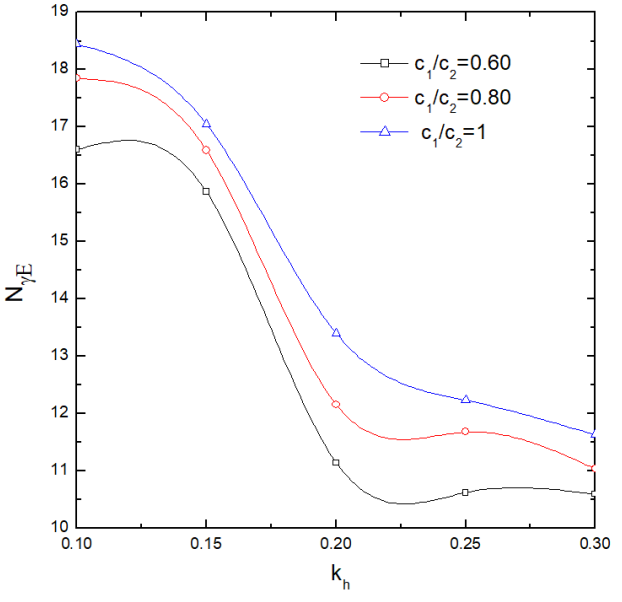

Figure 18: Variation of $N_{\gamma E}$ with k_h for $\phi_2 = 30°$, $\delta_2 = \phi_2/2$ $i = 15^0$, $\delta_1/\delta_2 = 0.8$, $k_V = k_h/2$, $\phi_1/\phi_2 = 0.8$, $D_f/B_0 = 0.5$, $h_1/B_0 = 0.25$, $\gamma_1/\gamma_2 = 0.8$.

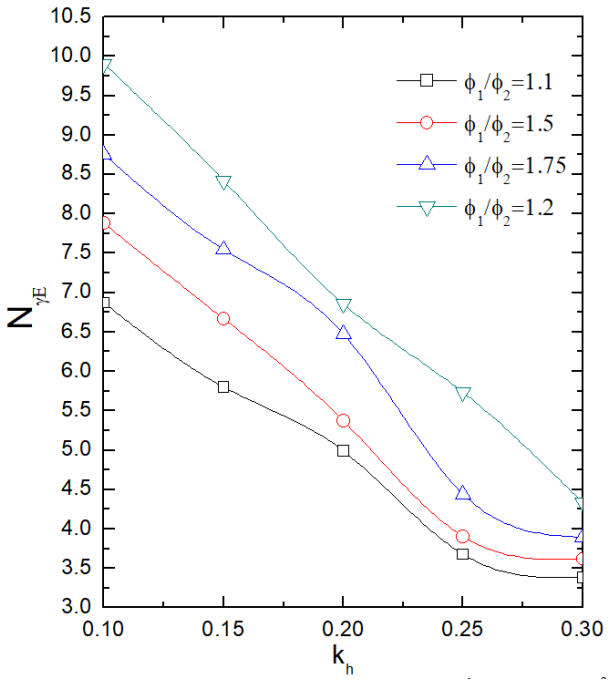

Figure 19: Variation of $N_{\gamma E}$ with k_h for $\phi_2 = 20°$, $\delta_2 = \phi_2/2$, i = 20° $\delta_1/\delta_2 = 1.1$, $k_v = k_h/2$, $\gamma_1/\gamma_2 = 1.1$, $D_f/B_0 = 0.50$, $2c_2/B_0\gamma_2 = 0$, $c_1/c_2 = 0$.

3.3.11 Variations of seismic bearing capacity coefficient for different values of using $\frac{\gamma_1}{\gamma_2}$ PSO algorithm

Figure 20 shows the variations of seismic bearing capacity coefficient $(N_{\gamma E})$ at $\phi_2 = 30^0$, $\delta_2 = \frac{\phi_2}{2}$, $\frac{h_1}{B_0} = 0.25$, $\frac{\delta_1}{\delta_2} = 1.1$, $k_v = \frac{k_h}{2}$, $\frac{\phi_1}{\phi_2} = 1.1$, $\frac{D_f}{B_0} = 0.5$, $\frac{2c_2}{\gamma_2 B_0} = 0$ and $\frac{c_1}{c_2} = 0$ with k_h. From the figure, it is seen that the coefficient $N_{\gamma E}$ increases with an increase in the value of $\frac{\gamma_1}{\gamma_2}$. The ratio $\frac{\gamma_1}{\gamma_2}$ is increased keeping γ_2 as a constant. Here, γ_1 is the unit weight of the strong soil layer and γ_2 is the unit weight of the weak soil layer.

3.3.12 Variations of seismic bearing capacity coefficient for different values of $\frac{c_1}{c_2}$ using PSO algorithm

Figure 21 shows the variations of $(N_{\gamma E})$ at $\phi_2 = 30^0$,$\delta_2 = \frac{\phi_2}{2}$, $\frac{h_1}{B_0} = 0.25$, $\frac{\delta_1}{\delta_2} = 1.1$, $k_v = \frac{k_h}{2}$, $\frac{\gamma_1}{\gamma_2} = 1.1$, $\frac{D_f}{B_0} = 0.5$, $\frac{2c_2}{\gamma_2 B_0} = 0.2$, $\frac{\phi_1}{\phi_2} = 0$ with k_h. From the plot, it is seen that the coefficient $N_{\gamma E}$ increases with an increase in the values of $\frac{c_1}{c_2}$. Here, c_2 is the cohesive force on the weak soil layer and c_1 is the cohesive force on the strong soil layer. Hence, the ratio $\frac{c_1}{c_2}$ is increased while keeping c_2 constant. So, the value $N_{\gamma E}$ will increase.

Table 3: Comparison of variation of seismic bearing capacity (q_{uE}) KN/m^2 with γ (KN/m^3) for the case of $\phi = 30^\circ, c = 9.8KN/m^2, i = 20^\circ, B_0 = 10m$.

	Sawada et al. (1994)		Askari and Farzaneh (2003)		Yamamoto (2010)		Present Analysis	
k_h	γ=9.8	γ=19.8	γ=9.8	γ=19.8	γ=9.8	γ=19.8	γ=9.8	γ=19.8
0.1	1798	3321	1066	1856	1013	1795	1614.14	3139.92
0.2	1770	3269	829	1307	755	1283	654	1167

Table 4: Comparison of the variation in N_{cs} with different $c_u/\gamma B_0$, D_f/B_0, c_1/c_2 for i=30°.

$c_u/\gamma B_0$	N_{cs} (Present study)				N_{cs} (Wu et al. 2020)			
	D_f/B_0=0.5, c_1/c_2=0.5	D_f/B_0=1.5, c_1/c_2=0.5	D_f/B_0=1.5, c_1/c_2=1.5	D_f/B_0=0.5, c_1/c_2=1.5	D_f/B_0=0.5, c_1/c_2=0.5	D_f/B_0=1.5, c_1/c_2=0.5	D_f/B_0=1.5, c_1/c_2=1.5	D_f/B_0=0.5, c_1/c_2=1.5
1	4.06	3.78	2.78	2.34	4.05	3.79	2.8	2.34
2	4.15	3.92	3.05	2.95	4.16	3.96	3.01	3.01
4	4.20	4.02	3.11	3.04	4.19	4.02	3.12	3.12
6	4.22	4.04	3.22	3.10	4.2	4.04	3.15	3.15
8	4.24	4.06	3.23	3.14	4.21	4.05	3.17	3.17
10	4.25	4.08	3.24	3.16	4.22	4.6	3.17	3.17

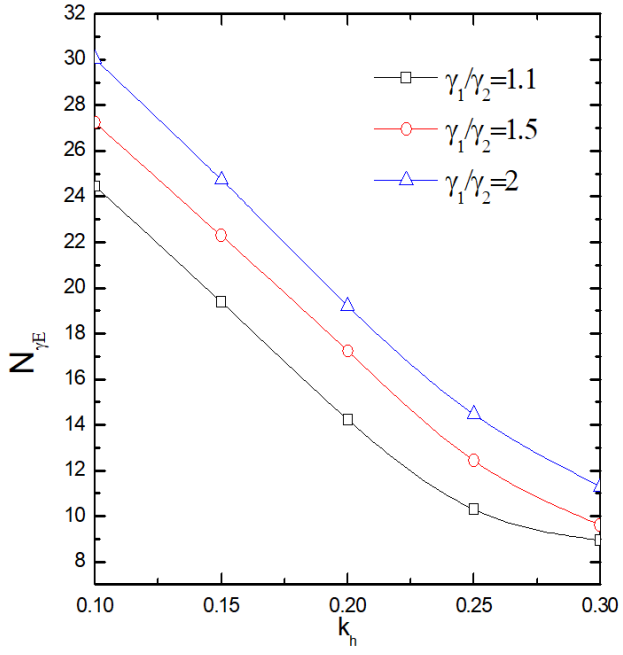

Figure 20: Variation of $N_{\gamma E}$ with k_h for $\phi_2 = 30^\circ, i = 20^\circ, \delta_2 = \phi_2/2$, $h_1/B_0 = 0.25, \delta_1/\delta_2 = 1.1, k_v = k_h/2, \phi_1/\phi_2 = 1.1, D/B_0 = 0.50, 2c_2/B_0\gamma_2 = 0, c_1/c_2 = 0$.

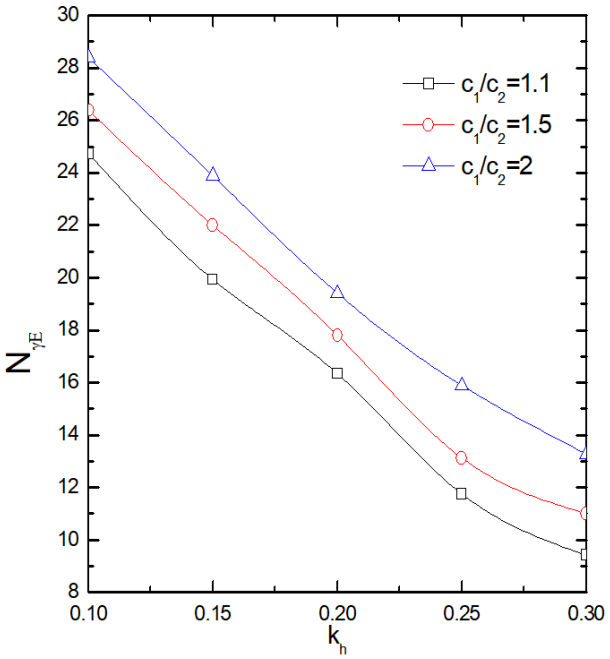

Figure 21: Variation of $N_{\gamma E}$ with k_h for $\phi_2 = 30^\circ$, i = 20°, $\delta_2 = \phi_2/2$, $h_1/B_0 = 0.25$, $\delta_1/\delta_2 = 1.1$, $k_v = k_h/2$, $\phi_1/\phi_2 = 1.1$, $D/B_0 = 0.50$, $\gamma_1/\gamma_2 = 1.1$.

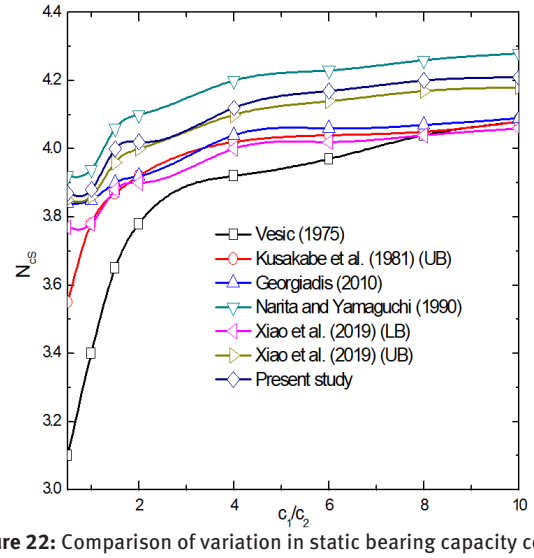

Figure 22: Comparison of variation in static bearing capacity coefficients (N_CS) with c_1/c_2 for $i = 30^0$.

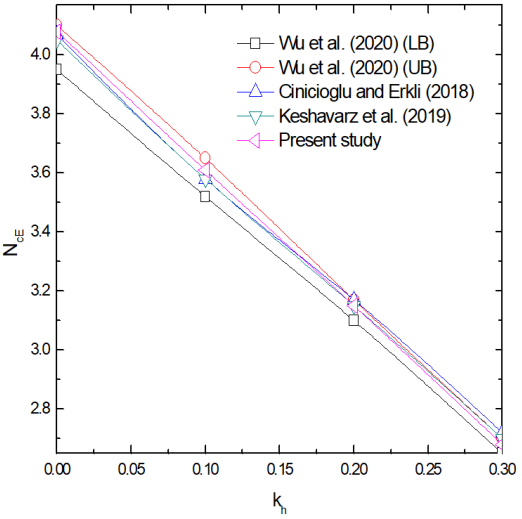

Figure 23: Comparison of seismic bearing capacity coefficients (N_{cE}) with k_h for $D_f/B_0 = 0, i = 30°, c_1/c_2 = 1$.

4 Comparisons

The bearing capacity coefficient $(N_{\gamma''})$ has been computed by using a computer programing software 'MATLAB' code. PSO algorithm is applied, which can calculate the ultimate bearing capacity, q_{ult}, for various combinations of soil properties in each layer. Table 3 shows a comparison of the ultimate bearing capacity for $D_f/B_0 = 0.25$ between Askari and Farzaneh (2003), Sawada et al. (1994), Yamamoto (2010) and the present analysis,demonstrating the potentiality of the present analysis. It is found that the solutions from Sawada et al. (1994) have high values with the increase of γ, compared with those from Askari and Farzaneh (2003), Yamamoto (2010) and the present analysis. This fact depends on the assumed failure mechanism. For the case of $\gamma = 9.8, 19.8$, the solutions from the present analysis tend to have lower values than those from Askari and Farzaneh (2003). The proposed solutions of the footing at two-layered slope with different $c_u/\gamma B_0$, D_f/B_0 and c_1/c_2 are compared with the results of Wu et al. (2020), as shown in Table 4. These results are compared for bearing capacity coefficient (N_{cs}). The undrained seismic bearing capacity coefficients can be written as: $N_{cs}=q_{ult}/c_1=f(c_u/\gamma B_0,\ D_f/B_0,\ c_1/c_2, i, k_h)$. q_{ult} is the ultimate bearing capacity of the strip footing. The cases of footings lying on two-layered level ground with the seismic action are compared with the results of Jahani et al. (2019), and the comparison is presented in Table 5. It is observed from Table 5 that the results of the present study agree well with those of previous studies. Consequently, Tables 6–8 display comparisons of the variation in N_{cs} with Xiao et al. (2019) for different slope angles i=15^0, 30^0 and 45^0. The undrained static bearing capacity factors for cohesion (N_{cs}) obtained in the present study for a footing of uniform slope were compared with the UB and LB solutions of Xiao et al. (2019), semi-empirical results reported by Vesic (1975), the upper bound (UB) solutions obtained from Kusakabe et al. (1981), the limit-equilibrium methods of Narita and Yamaguchi (1990) and the finite element results provided by Georgiadis (2010). Comparison of these results is shown in Fig. 22 for the case of slope angle (i)=30^0. In Fig. 22, it is observed that the values of N_{cs} obtained from the UB solutions of Kusakabe et al. (1981) and Georgiadis (2010) lie between the UB and LB solutions of Xiao et al. (2019). The semi-empirical solutions of Vesic (1975) give the lowest values, whereas the values reported by Narita and Yamaguchi (1990) are found to be the highest dimensionless bearing capacity coefficients. From this figure, it is also observed that the values obtained in the present study are closer to the UB solutions obtained by Xiao et al. (2019) and Narita and Yamaguchi (1990). The present values lie between these two researches' values. To verify the reliability of the present model, the LB and UB results were compared with the present limit equilibrium method. The present model of $D_f/B_0 = 0$, $i = 30^0$ and$c_1/c_2 = 1$ with different seismic coefficients k_h were compared with the previous LB and UB results (Wu et al. 2020), FEM results (Cinicioglu and Erkli 2018) and FELA results (Keshavarz et al. 2019). It can be seen in Fig. 23 that the present seismic bearing capacity coefficients (N_{cE}) closely match with the Upper bound (UB) limit analysis values.Based on the comparisons mentioned above, the proposed model can be proved with relatively minor error.

Table 5: Comparison of the variation in N_{cs} with different k_h and c_1/c_2 for i=0° and D_f/B_0.

	N_{cs} (Present study)			N_{cs} (Jahani et al. 2019)		
k_h	c_1/c_2=0.25	c_1/c_2=0.50	c_1/c_2=0.75	c_1/c_2=0.25	c_1/c_2=0.50	c_1/c_2=0.75
0	5.62	3.94	3.06	5.67	4	3.1
0.1	5.20	3.48	2.75	5.25	3.58	2.73
0.2	4.04	3.04	2.37	4.44	3.12	2.4
0.3	3.38	2.65	2.12	3.47	2.7	2.15

Table 6: Comparison of the variation in N_{cs} for i=15°.

h_1/B_0	D_f/B_0	c_1/c_2	Xiao et al. (2019)				Present study			
			$c_1/\gamma B_0$				$c_1/\gamma B_0$			
			1	2	4	6	1	2	4	6
0.5	0.25	0.25	5.71	5.73	5.74	5.74	5.68	5.70	5.71	5.72
		0.5	5.71	5.73	5.74	5.74	5.68	5.70	5.71	5.72
		0.75	5.53	5.57	5.58	5.59	5.49	5.55	5.56	5.57
		1	4.51	4.58	4.61	4.63	4.49	4.53	4.58	4.60
	0.50	0.25	4.70	4.75	4.77	4.77	4.68	4.71	4.74	4.74
		0.5	4.70	4.75	4.77	4.77	4.68	4.72	4.75	4.75
		0.75	4.70	4.74	4.77	4.77	4.68	4.71	4.75	4.75
		1	4.51	4.57	4.61	4.62	4.45	4.51	4.59	4.59
1	0.25	0.25	5.71	5.73	5.73	5.75	5.68	5.70	5.71	5.72
		0.5	5.71	5.73	5.73	5.74	5.68	5.70	5.70	5.71
		0.75	5.52	5.57	5.58	5.59	5.50	5.55	5.56	5.57
		1	4.51	4.58	4.61	4.63	4.48	4.55	4.59	4.61
	0.50	0.25	4.70	4.75	4.77	4.78	4.68	4.72	4.74	4.75
		0.5	4.71	4.75	4.77	4.78	4.67	4.74	4.75	4.76
		0.75	4.70	4.75	4.77	4.78	4.66	4.74	4.74	4.75
		1	4.51	4.58	4.62	4.62	4.49	4.55	4.60	4.61
2	0.25	0.25	5.71	5.73	5.74	5.73	5.69	5.72	5.72	5.73
		0.5	5.71	5.73	5.74	5.74	5.69	5.71	5.72	5.73
		0.75	5.52	5.57	5.58	5.59	5.50	5.55	5.56	5.57
		1	4.51	4.58	4.62	4.63	5.49	5.53	5.54	5.55
	0.50	0.25	4.70	4.74	4.77	4.79	4.69	4.72	4.75	4.77
		0.5	4.70	4.76	4.77	4.77	4.68	4.70	4.73	4.75
		0.75	4.70	4.74	4.76	4.78	4.67	4.68	4.70	4.72
		1	4.51	4.58	4.61	4.62	4.47	4.54	4.59	4.60
3	0.25	0.25	5.70	5.73	5.74	5.74	5.69	5.71	5.72	5.72
		0.5	5.70	5.73	5.74	5.74	5.69	5.71	5.72	5.72
		0.75	5.52	5.56	5.58	5.58	5.50	5.55	5.56	5.57
		1	4.51	4.58	4.61	4.62	4.48	4.55	4.58	4.60
	0.50	0.25	4.71	4.75	4.77	4.78	4.69	4.72	4.74	4.77
		0.5	4.70	4.75	4.77	4.78	4.68	4.72	4.74	4.77
		0.75	4.70	4.75	4.77	4.77	4.67	4.71	4.73	4.73
		1	4.51	4.58	4.61	4.63	4.49	4.55	4.59	4.60

Table 7: Comparison of the variation in N_{cs} for i=30°.

h_1/B_0	D_f/B_0	c_1/c_2	Xiao et al. (2019)				Present study			
			$c_1/\gamma B_0$				$c_1/\gamma B_0$			
			1	2	4	6	1	2	4	6
0.5	0.25	0.25	5.15	5.20	5.23	5.23	5.11	5.16	5.21	5.21
		0.5	5.15	5.20	5.22	5.23	5.11	5.16	5.21	5.20
		0.75	4.86	4.95	5.00	5.01	4.81	4.88	4.91	4.96
		1	3.88	4.01	4.07	4.09	3.82	4.01	4.03	4.05
	0.50	0.25	4.09	4.18	4.23	4.24	4.05	4.16	4.20	4.21
		0.5	4.09	4.18	4.23	4.24	4.02	4.14	4.18	4.20
		0.75	4.09	4.18	4.23	4.24	4.01	4.12	4.16	4.18
		1	3.88	4.00	4.07	4.09	3.84	3.95	4.02	4.05
1	0.25	0.25	5.15	5.20	5.22	5.23	5.10	5.15	5.20	5.21
		0.5	5.15	5.20	5.22	5.23	5.09	5.13	5.19	5.20
		0.75	4.85	4.95	5.00	5.01	4.80	4.85	4.90	4.93
		1	3.83	3.99	4.06	4.08	3.80	3.92	3.99	4.01
	0.50	0.25	4.10	4.19	4.24	4.25	4.07	4.11	4.20	4.22
		0.5	4.10	4.19	4.23	4.25	4.05	4.10	4.19	4.20
		0.75	4.10	4.19	4.23	4.25	4.04	4.10	4.18	4.19
		1	3.83	3.99	4.06	4.08	3.80	3.95	4.04	4.06
2	0.25	0.25	5.15	5.20	5.22	5.23	5.11	5.17	5.20	5.21
		0.5	5.15	5.20	5.22	5.23	5.10	5.17	5.20	5.21
		0.75	4.85	4.95	5.00	5.01	4.82	4.90	4.96	4.99
		1	3.83	3.99	4.06	4.08	3.81	3.95	4.01	4.04
	0.50	0.25	4.09	4.19	4.23	4.25	4.07	4.15	4.20	4.22
		0.5	4.09	4.19	4.23	4.25	4.05	4.14	4.20	4.21
		0.75	4.09	4.19	4.23	4.25	4.05	4.14	4.20	4.21
		1	3.82	3.98	4.05	4.07	3.80	3.94	4.01	4.04
3	0.25	0.25	5.16	5.20	5.22	5.23	5.11	5.18	5.20	5.21
		0.5	5.16	5.20	5.22	5.23	5.11	5.17	5.20	5.21
		0.75	4.85	4.95	5.00	5.01	4.81	4.92	4.99	5.00
		1	3.83	3.99	4.06	4.08	3.80	3.96	4.03	4.06
	0.50	0.25	4.10	4.19	4.23	4.25	4.07	4.15	4.20	4.23
		0.5	4.09	4.19	4.23	4.24	4.06	4.14	4.20	4.22
		0.75	4.10	4.19	4.23	4.24	4.05	4.12	4.18	4.20
		1	3.83	3.99	4.06	4.08	3.80	3.93	4.03	4.06

Table 8: Comparison of the variation in N_{cs} for i=45°.

h_1/B_0	D_f/B_0	c_1/c_2	Xiao et al. (2019)				Present study			
			$c_1/\gamma B_0$				$c_1/\gamma B_0$			
			1	2	4	6	1	2	4	6
0.5	0.25	0.25	4.57	4.63	4.66	4.67	4.54	4.60	4.62	4.64
		0.5	4.57	4.64	4.66	4.68	4.53	4.60	4.61	4.63
		0.75	4.23	4.34	4.40	4.41	4.21	4.31	4.37	4.40
		1	3.44	3.57	3.63	3.65	3.41	3.53	3.55	3.59
	0.50	0.25	3.49	3.62	3.67	3.70	3.45	3.58	3.62	3.67
		0.5	3.49	3.61	3.67	3.70	3.44	3.59	3.60	3.67
		0.75	3.49	3.61	3.68	3.70	3.43	3.56	3.59	3.66
		1	3.44	3.57	3.63	3.65	3.42	3.53	3.56	3.64
1	0.25	0.25	4.57	4.63	4.66	4.67	4.55	4.60	4.63	4.65
		0.5	4.57	4.63	4.66	4.68	4.54	4.58	4.62	4.64
		0.75	4.13	4.28	4.35	4.37	4.11	4.25	4.33	4.35
		1	3.16	3.41	3.51	3.54	3.11	3.38	3.50	3.52
	0.50	0.25	3.49	3.61	3.68	3.69	3.45	3.59	3.64	3.67
		0.5	3.49	3.61	3.68	3.69	3.44	3.58	3.63	3.67
		0.75	3.49	3.61	3.68	3.69	3.43	3.57	3.63	3.67
		1	3.16	3.41	3.51	3.54	3.12	3.38	3.50	3.52
2	0.25	0.25	4.58	4.64	4.66	4.68	4.54	4.60	4.62	4.66
		0.5	4.58	4.63	4.67	4.68	4.53	4.60	4.61	4.64
		0.75	4.11	4.28	4.35	4.38	4.10	4.25	4.32	4.32
		1	3.15	3.41	3.50	3.54	3.11	3.40	3.48	3.50
	0.50	0.25	3.49	3.61	3.67	3.69	3.44	3.58	3.62	3.64
		0.5	3.49	3.61	3.68	3.69	3.42	3.56	3.61	3.63
		0.75	3.49	3.61	3.67	3.69	3.41	3.54	3.58	3.61
		1	3.15	3.41	3.51	3.54	3.10	3.36	3.52	3.52
3	0.25	0.25	4.58	4.64	4.67	4.67	4.55	4.62	4.64	4.65
		0.5	4.58	4.63	4.67	4.68	4.54	4.60	4.62	4.64
		0.75	4.11	4.28	4.35	4.37	4.08	4.24	4.31	4.35
		1	3.15	3.40	3.51	3.54	3.12	3.36	3.41	3.48
	0.50	0.25	3.49	3.61	3.67	3.69	3.44	3.60	3.62	3.65
		0.5	3.48	3.61	3.67	3.69	3.43	3.60	3.61	3.63
		0.75	3.49	3.61	3.67	3.67	3.42	3.58	3.60	3.63
		1	3.15	3.40	3.51	3.54	3.13	3.38	3.49	3.51

5 Conclusions

This paper has investigated the seismic bearing capacity of shallow foundations near slope using pseudo-static limit equilibrium analysis. Linear failure mechanism has been proposed to obtain pseudo-static bearing capacity coefficients of embedded strip footing near slope using limit equilibrium analysis. The PSO technique has been applied to obtain minimum bearing capacity coefficients.

Based on the present investigation, the following conclusions can be drawn:

1. $N_{\gamma E}$ values from the present analysis agreed well with other analyses reported by Askari and Farzaneh (2003), Sawada et al. (1994) and Yamamoto (2010). The present analysis shows a tendency to decrease $N_{\gamma E}$ values by increasing the horizontal seismic coefficient (k_h) and vertical seismic coefficient (k_v).
2. The seismic bearing capacity coefficient N_{cs} was found relatively minor error value with previous researchers.
3. The minimum pseudo-static bearing capacity coefficients are presented in the form of design table for practical use in geotechnical engineering. It has been observed that the magnitude of bearing capacity coefficients decreases with an increase in slope inclination.
4. The seismic bearing capacity decreases with greater undrained shear strength ratio (c_1/c_2) and the effect becomes more significant when the thickness of the top layer decreases.
5. The value of N_{cs} increases with increasing $c_1/\gamma B_0$, whereas thiseffect recedes with an increase of $c_1/\gamma B_0$. Also,greater value of $c_1/\gamma B$ would decrease the effect of bottom layer.

Data availability statement: The authors confirm that some data and code generated during this study are proprietary or confidential and may only be provided with restrictions (e. g., PSO code).

References

Aote, S. S., Raghuwanshi, M. M., & Malik, L. (2013). A brief review of particle swarm optimization: limitations & future directions. *International Journal of Computer Science Engineering* (IJCSE), 2(5), 196-200.

Askari, F., and Farzaneh, O. (2003), "Upper-bound solution for Seismic bearing capacity of shallow foundation near slopes", *Geotechniqe*53(8), 697-702.

Baazouzi, M., Benmeddour, D., Mabrouki, A., and Mellas, M. (2016), " 2D numerical analysis of shallow foundation rested near slope under inclined loading", *Procedia Engineering*, Elsevier, 143, 623-634.

Budhu, M., and Al-Karni, A. (1993), "Seismic bearing capacity of soils", *Geotechnique*43(1): 181-187.

Button, S.J. (1953). "The bearing capacity of footings on two-layer cohesive subsoil." Proc. 3rd Intl. Conference on Soil Mechanics and Foundation Engrg., 1, Zurich: 332-335.

Castelli, F. and Lentini, V. (2012) Evaluation of the bearing capacity of footings on a slope. *Int J Phys Model GeotechEng*12(3):112-118

Chakraborty, D., and Kumar, J., (2013), " Bearing Capacity of Foundations on slopes", *Geomechanics and Geoengineering,*8(4), 274-285.

Chakraborty, D., and Kumar, J., (2014), " Seismic Bearing Capacity of Shallow strip Footing Embedded in slope", *International Journal of Geomechanics*,6: 176-184

Cheng, Y. M., Li, L., and Chi, S. C. (2007). "Performance studies on six heuristic global optimization methods in the location ofcritical slip surface". *ComputGeotech.,* 34(6):462–484. DOI:10.1016/j.compgeo.2007.01.004.

Choudhury, D., and Subba Rao, K. S. (2006), " Seismic bearing capacity of foundations on slopes". *Geotechnique,* 53(3), 347-361

Choudhury, D., SubhaRao, K. S. (2005), " Seismic uplift capacity of inclined slip anchors", *Can Geotech. J.,* 42(1), 263-271.

Debnath, L. and Ghosh, S. (2018), "Pseudo-static analysis of shallow strip footingresting on two layered soil", *International Journal of Geomechanics*, ASCE, doi:10.1061/(ASCE)GM.1943-5622.0001049.

Dormieux, L., and Pecker, A. (1995). " Seismic bearing capacity of foundations on cohesionless soil", *J. Geotech. Eng.,* ASCE, 121(3), 300-303

Engelbrecht AP (2007) Computational intelligence: an introduction.Wiley, London

Farzaneh O, Mofidi J, Askari F (2013) Seismic bearing capacity of strip footings near cohesive slopes using lower bound limit analysis. In: Proceedings of the 18th international conference on soil mechanics and geotechnical engineering, Paris, pp 1467-1470

Gbenga, D. E., &Ramlan, E. I. (2016). Understanding the limitations of the particle swarm algorithm for dynamic optimization tasks: A survey towards the singularity of PSO for swarm robotic applications. *ACM Computing Surveys* (CSUR), 49(1), 8.

Hajihassani,M., Armaghani, J. D. and Kalatehjari, R. (2017). "Applications of Particle Swarm Optimizationin Geotechnical Engineering: A Comprehensive Review", Geotech. Geol. Eng. , Springer, DOI 10.1007/s10706-017-0356-z.

Hossain MS, El-Shafie A (2014) Evolutionary techniques versus swarm intelligence: application in reservoir release optimization. *Neural ComputAppl* 24(7):1583–1594. doi:10.

IS 1893-1984(Part 3), "Indian Standard Criteria for Earthquake Resistant Design of Structures", *Bureau of Indian Standards,* New Delhi.

Kalatehjari, R. (2013)."An improvised three-dimensional slope stability analysis based on limit equilibrium method by using particle swarm optimization". Dissertation, UniversitiTeknologi Malaysia.

Kennedy, J., and Eberhart, R. (1995). "Particle swarm optimization", *In Proceedings of IEEE international conference on neural networks* 4, pp.1942–1948.

Kumar, J. (2003), " Nγ for rough strip footing using the method of characteristics", *Can. Geotech. J.,* 40(3), 669-674

Kumar, J., and Ghosh, P. (2006). "Seismic bearing capacity for embedded footings on sloping ground." Geotechnique, 56(2), 133-140.

Kumar, J. and Kumar, N. (2003), " Seismic bearing capacity of rough footings on slopes using limit equilibrium", *Geotechnique,* 53(3), 3*63-369*

Kumar, J., and Rao, V. B.K. M. (2002), " Seismic bearing capacity factors for spread foundations", *Geotechnique,* 52(2), 79-88

Meyerhof, G. G. (1957), "The ultimate bearing capacity of foundation on slopes", *In Proc. of 4th Int. Conf. on Soil Mech. and Found. Engg.,* London 1, 384-386

Meyerhof, G. G., and Hanna, A. M. (1978). Ultimate bearing capacity of foundations on layered soils under inclined load. *Canadian Geotechnical Journal*, 15(4), 565-572.

Michalowski, R. L., and Shi, L. (1995). Bearing capacity of footings over two-layer foundation soils. *Journal of Geotechnical Engineering*, 121(5), 421-428.

Mononobe, N., and Matsuo, H. (1929), "*On the* Determination of Earth pressure during Earthquakes", *Proc. of the World Engineering Congress,* Tokyo, *9*, 179-87

Mononobe, N., and Matsuo, H. (1929). On the determination of earth pressure during earthquakes: Proceedings of the World Engineering Congress.

Okabe, S. (1924). The general theory on earth pressure and seismic stability of retaining wall and dam. Proc. Civil Engrg. Soc., Japan, 10(6), 1277-1323.

Paolucci, R. and Pecker, A. (1997), "Seismic bearing capacity of shallow strip foundations on dry soils", *Soils Found., 37(3),* 95-105

Prandtl, L. (1921), " Umber die eindringungkeit plasticizer baustoffe und die festigkeit von schneiden", *Zeitschrift Fur Angewandt-Mathematik Und Mechanik,* 1 (1), 15-30 (in German)

Purushothamaraj, P., Ramiah, B.K., and Venkatakrishna, K.N. (1974). "Bearing capacity of strip footings in two-layered cohesive-friction soils." *Can. Geotech. J.*, 11: 32-45

Rankine, W. J. M. (1857), " On the stability of Loose Earth", *Phil. Tras. Royal Society* (London)

Reynolds CW (1987) Flocks, herds, and schools: a distributedbehavioral model. *ACM SIGGRAPH Comput Gr*21(4):25–34

Richards, R., Elms, D. G., and Budhu, M. (1993). " Seismic Bearing Capacity and Settlement of Foundations", *J. Geotech. Eng.,* ASCE, 119(4): 662-674.

Saran, S., Sud, V. K., and Handa, S. C. (1989), "Bearing capacity of footings adjacent to slopes", *J. Geotech. Eng.,* 115(4), 553-573

Sarma, S. K. (1999), " Seismic bearing capacity of shallow strip footings adjacent to a slope", *Proc., 2nd Int. Conf. Earthquake Geotechnical Engineering,* Lisbon, Portugal, Balkema, Rotterdam, The Netherlands, 309-313.

Sarma, S. K., and lossifelis, I. S. (1990), " Seismic bearing capacity factors of shallow strip footings", *Geotechnique,* 402, 265-273.

Sawada, T., Nomachi, S. G., and Chen, W. F. (1994), "Seismic bearing capacity of a mounded foundation near a downhill slope by pseudo-static analysis", *Soils Found.,* 34(1), 11-17.

Soubra, A. H. (1999), " Upper bound solutions for bearing capacity of foundations", *J. Geotech. Geotech. Geoenviron. Eng.,* ASCE 125 (1): 59-69.

Terzaghi, K. (1943), " Theoretical Soil Mechanics", *Wiley*

Yamamoto, K. (2010), "Seismic bearing capacity of shallow foundations near slopes using the upper-bound method", *Int. J. Geotech. Engg.,* 4, 255-267.

Zhu, D. Y. (2000), "The least upper-bound solutions for bearing capacity factorNγ", *Soils. Found.,* 40(1), 123-129.

Jahani, M., Oulapour, M, andHaghighi, A.(2019)."Evaluation of the seismic bearing capacity ofshallow foundations located on the two-layered clayey soils."*Iran J SciTechnol Trans Civ Eng*. 43(1):49–57.

Xiao Y, et al.(2019)."Undrained bearing capacity of strip footings placed adjacent to twolayered slopes." *Int. J. Geomech*;19(8).Doi:

Merifield, R. S., S. W. Sloan, and H. S. Yu. (1999). "Rigorous plasticity solutionsfor the bearing capacity of two-layered clays." *Geotechnique* 49 (4): 471–490. https://doi.org/10.1680/geot.1999.49.4.471.

Wu,G., Zhao, H., Zhao, M, and Xiao, Y. (2020). " Undrained seismic bearing capacity of strip footing lying on two-layered slopetwo-layered slopes." *Computer and Geotechnique* 122: https://doi.org/10.1016/j.compgeo.2020.103539.

Vesic, A. S. (1975). "Bearing capacity of shallow foundations." In Foundation engineering handbook, edited by H. F. Winterkorn andH. Y. Fang, 144–165. New York: Van Nostrand Reinhold.

Kusakabe, O., T. Kimura, and H. Yamaguchi. (1981). "Bearing capacity of slopes under strip loads on the top surfaces." Soils. Found. 21 (4): 29–40. .

Georgiadis, K. (2010). "Undrained bearing capacity of strip footings on slopes." J. Geotech. Geoenviron. Eng. 136 (5): 677–685. .

Narita, K., and H. Yamaguchi. (1990). "Bearing capacity analysis of foundations on slopes by use of log-spiral sliding surfaces." Soils Found. 30(3): 144–152. .

Xiao, Y., Zhao, M., Zhang, R., Zhao, H. and Wu, G. (2019). "Undrained Bearing Capacity of Strip Footings PlacedAdjacent to Two-Layered Slopes." Int. J. Geomech., ASCE, Doi: 10.1061/(ASCE)GM.19435622.0001480.

Cinicioglu, O. and Erkli, A. (2018)."Seismic bearing capacity of surficial foundations on sloping cohesive ground." Soil Dynamics and Earthquake Engineering, 111: 53–64.

Keshavarz, A., Beygi, M. and Vali, R. (2019)."Undrained seismic bearing capacity of strip footing placed on homogeneous and heterogeneous soil slopes by finite element limit analysis." Computers and Geotechnics, 113: 103094.

Wu, G., Eeri, M., Zhao, M. and Zhao, H. (2020). "Undrained seismic bearingcapacity of strip footingshorizontally embedded intwo-layered slopes." Earthquake Spectra, DOI: 10.1177/8755293020957332.

A Appendix I

$$P_{A1} = \frac{p_L B_0}{B_0 + \boldsymbol{h}_1}\left(B_0 - \boldsymbol{h}_1 \cot \alpha_{A1}\right)$$
$$\left\{\frac{(1-k_v)\sin(\alpha_{A2}-\phi_2) + k_h \tan\phi_1 \cos(\alpha_{A2}-\phi_2)}{\cos(\alpha_{A2}-\phi_2-\delta_2)}\right\}$$
$$+\frac{1}{2}\left(B_0 - \boldsymbol{h}_1 \cot \alpha_{A1}\right)\boldsymbol{h}_2\gamma_2$$
$$\left\{\frac{(1-k_v)\sin(\alpha_{A2}-\phi_2) + k_h \cos(\alpha_{A2}-\phi_2)}{\cos(\alpha_{A2}-\phi_2-\delta_2)}\right\}$$
$$+\gamma_1 \boldsymbol{h}_1\left(B_0 - \boldsymbol{h}_1 \cot \alpha_{A1}\right)$$

$$\left\{\frac{(1-k_v)\sin(\alpha_{A2}-\phi_2)+k_h\tan\phi_1\cos(\alpha_{A2}-\phi_2)}{\cos(\alpha_{A2}-\phi_2-\delta_2)}\right\}$$
$$-2c_2\boldsymbol{h}_2\frac{\sin(\alpha_{A2}-\phi_2)}{\cos(\alpha_{A2}-\phi_2-\delta_2)}$$
$$-c_2\boldsymbol{h}_2\cot\alpha_{A2}\frac{\cos(\alpha_{A2}-\phi_2)}{\cos(\alpha_{A2}-\phi_2-\delta_2)}$$
$$-c_1\left[\boldsymbol{h}_1\cot\alpha_{A1}\frac{\cos(\alpha_{A2}-\phi_2)}{\cos(\alpha_{A2}-\phi_2-\delta_2)}-B_0\frac{\cos(\alpha_{A2}-\phi_2)}{\cos(\alpha_{A2}-\phi_2-\delta_2)}\right]$$

$$P_{p2}=\frac{1}{2}h_2^2\cot\alpha_{p2}\gamma_2$$
$$\left\{\frac{(1-k_v)\sin(\phi_2+\alpha_{p2})-k_h\cos(\phi_2+\alpha_{p2})}{\cos(\phi_2+\alpha_{p2}+\delta_2)}\right\}$$
$$+\gamma_1h_1h_2\cot\alpha_{p2}$$
$$\left\{\frac{(1-k_v)\sin(\phi_2+\alpha_{p2})+k_h\tan\phi_1\cos(\phi_2+\alpha_{p2}))}{\cos(\phi_2+\alpha_{p2}+\delta_2)}\right\}$$
$$+\gamma_1D_f\frac{(h_1\cot\alpha_{p1}+h_2\cot\alpha_{p2})}{(h_1+h_1\cot\alpha_{p1}+h_2\cot\alpha_{p2})}h_2\cot\alpha_{p2}$$
$$\left\{\frac{(1-k_v)\sin(\phi_2+\alpha_{p2})+k_h\tan\phi_1\cos(\phi_2+\alpha_{p2})}{\cos(\phi_2+\alpha_{p2}+\delta_2)}\right\}$$
$$+2c_2h_2\left\{\frac{\sin(\phi_2+\alpha_{p2})}{\cos(\phi_2+\alpha_{p2}+\delta_2)}\right\}+$$
$$c_1h_2\cot\alpha_{p2}\left\{\frac{\cos(\phi_2+\alpha_{p2})}{\cos(\phi_2+\alpha_{p2}+\delta_2)}\right\}+$$
$$c_2h_2\cot\alpha_{p2}\left\{\frac{\cos(\phi_2+\alpha_{p2})}{\cos(\phi_2+\alpha_{p2}+\delta_2)}\right\}$$

B Appendix II

$$a_1=\frac{\gamma_1}{\bar{\gamma}}\left\{\begin{array}{c}\left(\frac{h_1}{B_0}\cot\alpha_{p1}+2\frac{h_2}{B_0}\cot\alpha_{p2}\right)\frac{h_1}{B_0}-\\ \frac{1}{4}\left(h_1\cot\alpha_{p1}+h_2\cot\alpha_{p2}-\frac{D_f}{\tan i}+\frac{B_0}{2}\right)^2\tan\alpha_{p1}\end{array}\right\}$$
$$\left\{\frac{(1-k_v)\sin(\phi_1+\alpha_{p1})-k_h\cos(\phi_1+\alpha_{p1})}{\cos(\phi_1+\alpha_{p1}+\delta_1)}\right\}$$
$$\left\{\frac{(1-k_v)\sin(\phi_1+\alpha_{p1})+k_h\tan\phi_2\cos(\phi_1+\alpha_{p1})}{\cos(\phi_1+\alpha_{p1}+\delta_1)}\right\}$$
$$+\left(\frac{h_2}{B_0}\right)^2\cot\alpha_{p2}\frac{\gamma_2}{\bar{\gamma}}$$
$$\left\{\frac{(1-k_v)\sin(\phi_2+\alpha_{p2})-k_h\cos(\phi_2+\alpha_{p2})}{\cos(\phi_2+\alpha_{p2}+\delta_2)}\right\}$$
$$+2\frac{\gamma_1}{\bar{\gamma}}\frac{h_1}{B_0}\frac{h_2}{B_0}\cot\alpha_{p2}$$
$$\left\{\frac{(1-k_v)\sin(\phi_2+\alpha_{p2})+k_h\tan\phi_2\cos(\phi_2+\alpha_{p2})}{\cos(\phi_2+\alpha_{p2}+\delta_2)}\right\}$$
$$-\left(2-\frac{h_1}{B_0}\cot\alpha_{A1}\right)\frac{h_1}{B_0}\frac{\gamma_1}{\bar{\gamma}}$$
$$\left\{\frac{(1-k_v)\sin(\alpha_{A1}-\phi_1)+k_h\cos(\alpha_{A1}-\phi_1)}{\cos(\alpha_{A1}-\phi_1-\delta_1)}\right\}$$
$$+2\frac{\gamma_1}{\bar{\gamma}}\frac{h_1}{B_0}\left(1-\frac{h_1}{B_0}\cot\alpha_{A1}\right)$$
$$\left\{\frac{(1-k_v)\sin(\alpha_{A1}-\phi_1)+k_h\tan\phi_2\cos(\alpha_{A1}-\phi_1)}{\cos(\alpha_{A1}-\phi_1-\delta_1)}\right\}$$
$$-\left(1-\frac{h_1}{B_0}\cot\alpha_{A1}\right)\frac{h_2}{B_0}\frac{\gamma_2}{\bar{\gamma}}$$
$$\left\{\frac{(1-k_v)\sin(\alpha_{A2}-\phi_2)+k_h\cos(\alpha_{A2}-\phi_2)}{\cos(\alpha_{A2}-\phi_2-\delta_2)}\right\}$$
$$-2\frac{\gamma_1}{\bar{\gamma}}\frac{h_1}{B_0}\left(1-\frac{h_1}{B_0}\cot\alpha_{A1}\right)$$
$$\left\{\frac{(1-k_v)\sin(\alpha_{A2}-\phi_2)+k_h\tan\phi_1\cos(\alpha_{A2}-\phi_2)}{\cos(\alpha_{A2}-\phi_2-\delta_2)}\right\}$$

$$b_1=2\frac{\gamma_1}{\bar{\gamma}}\tan i\left(\frac{D_f}{B_0\tan i}-\frac{1}{2}\right)^2$$
$$\left\{\frac{(1-k_v)\sin(\phi_1+\alpha_{p1})-k_h\cos(\phi_1+\alpha_{p1})}{\cos(\phi_1+\alpha_{p1}+\delta_1)}\right\}$$
$$-2\frac{\gamma_1}{\bar{\gamma}}\frac{h_2}{B_0}\cot\alpha_{p2}\frac{\tan\left(\frac{D_f}{B_0}-\frac{1}{2}\right)2\left(\frac{D_f}{B_0}-\tan i\right)}{\left\{2\frac{D_f}{B_0}+\tan\left(2\frac{h_1}{B_0}-1\right)\right\}}$$
$$\left\{\frac{(1-k_v)\sin(\phi_1+\alpha_{p1})+k_h\tan\phi_2\cos(\phi_1+\alpha_{p1})}{\cos(\phi_1+\alpha_{p1}+\delta_1)}\right\}$$
$$+2\frac{\gamma_1}{\bar{\gamma}}\frac{h_2}{B_0}\cot\alpha_{p2}\frac{\tan\left(\frac{D_f}{B_0}-\frac{1}{2}\right)2\left(\frac{D_f}{B_0}-\tan i\right)}{\left\{2\frac{D_f}{B_0}+\tan\left(2\frac{h_1}{B_0}-1\right)\right\}}$$
$$\left\{\frac{(1-k_v)\sin(\phi_2+\alpha_{p2})+k_h\tan\phi_1\cos(\phi_2+\alpha_{p2})}{\cos(\phi_2+\alpha_{p2}+\delta_2)}\right\}$$

$$d_1=2\frac{c_2}{\bar{c}}\frac{h_2}{B_0}\frac{\sin(\phi_2+\alpha_{p2})}{\cos(\phi_2+\alpha_{p2}+\delta_2)}+$$
$$\frac{c_1}{\bar{c}}\frac{h_2}{B_0}\cot\alpha_{p2}\frac{\cos(\phi_2+\alpha_{p2})}{\cos(\phi_2+\alpha_{p2}+\delta_2)}+$$
$$\frac{c_2}{\bar{c}}\frac{h_2}{B_0}\cot\alpha_{p2}\frac{\cos(\phi_2+\alpha_{p2})}{\cos(\phi_2+\alpha_{p2}+\delta_2)}$$
$$+\frac{c_1}{\bar{c}}\frac{h_1}{B_0}\frac{\sin(\phi_1+\alpha_{p1})}{\cos(\phi_1+\alpha_{p1}+\delta_1)}$$
$$+\frac{c_1}{\bar{c}}\sin\alpha_{p1}\{\frac{h_1}{2B_0}\cos ec\alpha_{p1}-\frac{h_2}{2B_0}\cot\alpha_{p2}\sec\alpha_{p1}+$$
$$\frac{1}{2}\frac{D_f}{B_0\tan i}\sec\alpha_{p1}-\frac{1}{4}\sec\alpha_{p1}\}$$

$$\frac{\sin\left(\phi_1+\alpha_{p1}\right)}{\cos\left(\phi_1+\alpha_{p1}+\delta_1\right)}+\frac{c_1}{\bar{c}}\cot\alpha_{p1}$$

$$\left\{\frac{h_1}{2B_0}\cos ec\alpha_{p1}-\frac{h_2}{2B_0}\cot\alpha_{p2}\sec\alpha_{p1}+\frac{1}{2}\frac{D_f}{B_0\tan i}\sec\alpha_{p1}-\frac{1}{4}\sec\alpha_{p1}\right\}$$

$$\frac{\cos\left(\phi_1+\alpha_{p1}\right)}{\cos\left(\phi_1+\alpha_{p1}+\delta_1\right)}-\frac{c_1}{\bar{c}}\frac{h_2}{B_0}\cot\alpha_{p2}\frac{\cos\left(\phi_1+\alpha_{p1}\right)}{\cos\left(\phi_1+\alpha_{p1}+\delta_1\right)}$$

$$+2\frac{c_1}{\bar{c}}\frac{h_1}{B_0}\frac{\sin\left(\alpha_{A1}-\phi_1\right)}{\cos\left(\alpha_{A1}-\phi_1-\delta_1\right)}+$$

$$\frac{c_1}{\bar{c}}\frac{h_1}{B_0}\cot\alpha_{A1}\frac{\cos\left(\alpha_{A1}-\phi_1\right)}{\cos\left(\alpha_{A1}-\phi_1-\delta_1\right)}$$

$$+\frac{c_2}{\bar{c}}\frac{\cos\left(\alpha_{A1}-\phi_1\right)}{\cos\left(\alpha_{A1}-\phi_1-\delta_1\right)}+$$

$$\frac{c_2}{\bar{c}}\frac{h_1}{B_0}\cot\alpha_{A1}\frac{\cos\left(\alpha_{A1}-\phi_1\right)}{\cos\left(\alpha_{A1}-\phi_1-\delta_1\right)}$$

$$+2\frac{c_2}{\bar{c}}\frac{h_2}{B_0}\frac{\cos\left(\alpha_{A2}-\phi_2\right)}{\cos\left(\alpha_{A2}-\phi_2-\delta_2\right)}$$

$$+\frac{c_1}{\bar{c}}\frac{\cos\left(\alpha_{A2}-\phi_2\right)}{\cos\left(\alpha_{A2}-\phi_2-\delta_2\right)}-$$

$$\frac{c_1}{\bar{c}}\frac{h_1}{B_0}\cot\alpha_{A1}\frac{\cos\left(\alpha_{A2}-\phi_2\right)}{\cos\left(\alpha_{A2}-\phi_2-\delta_2\right)}$$

$$e_1=\left\{\frac{(1-k_v)\sin\left(\alpha_{A1}-\phi_1\right)+k_h\cos\left(\alpha_{A1}-\phi_1\right)}{\cos\left(\alpha_{A1}-\phi_1-\delta_1\right)}\right\}$$

$$-\left\{\frac{\left(1-\frac{h_1}{B_0}\cot\alpha_{A1}\right)}{1+\frac{h_1}{B_0}}\right\}$$

$$\left\{\frac{(1-k_v)\sin\left(\alpha_{A1}-\phi_1\right)+k_h\tan\phi_2\cos\left(\alpha_{A1}-\phi_1\right))}{\cos\left(\alpha_{A1}-\phi_1-\delta_1\right)}\right\}$$

$$+\left\{\frac{\left(1-\frac{h_1}{B_0}\cot\alpha_{A1}\right)}{1+\frac{h_1}{B_0}}\right\}$$

$$\left\{\frac{(1-k_v)\sin\left(\alpha_{A2}-\phi_2\right)+k_h\tan\phi_1\cos\left(\alpha_{A2}-\phi_2\right)}{\cos\left(\alpha_{A2}-\phi_2-\delta_2\right)}\right\}$$